

**Laboratory Testing of a Substrate Mechanism for
Decay Inhibition and Exceptional Preservation**

Author: Robert T. Young

Advisor: Derek Briggs

Second Reader: Pincelli Hull

Date: December 20, 2013

A Senior Essay presented to the faculty of the Department of Geology and Geophysics, Yale University, in partial fulfillment of the Bachelor's Degree.

In presenting this essay in partial fulfillment of the Bachelor's Degree from the Department of Geology and Geophysics, Yale University, I agree that the department may make copies or post it on the departmental website so that others may better understand the undergraduate research of the department. I further agree that extensive copying of this thesis is allowable only for scholarly purposes. It is understood, however, that any copying or publication of this thesis for commercial purposes or financial gain is not allowed without my written consent.

Robert Toshiro Young, 20 December, 2013

Laboratory Testing of a Substrate Mechanism for Decay Inhibition and Exceptional Preservation

Robert T. Young

Department of Geology and Geophysics, Yale University, New Haven, Connecticut, 06520

Abstract

In general, exceptional fossilization requires the inhibition of organic decay, the promotion of authigenic mineralization, or both. Substrate permeability and chemistry, which have long been hypothesized as important controls on such processes, were experimentally modeled in order to test their effects on organic preservation. Standardized masses of muscle tissue (cod: *Gadus morhua*) were buried in five different substrates: glass beads of three sizes, illite, and kaolinite. The experiments were regularly monitored for one month with infrared gas analysis (IRGA), which quantified the carbon dioxide emitted by each sample and provided a proxy for decay rate. The resultant data revealed a strong positive association between substrate permeability and decay: samples buried in coarse beads emitted more carbon dioxide and reached a maximum emissions rate earlier than samples buried in fine beads. Samples buried in clay evidenced intermediate decay rates: kaolinite replicates emitted more carbon dioxide than their illite counterparts but achieved a maximum emissions rate simultaneously with them. These results indicate that preservation potential is maximized by low permeability conditions that restrict oxidant diffusion; they also suggest that decay rate is sensitive to different chemical environments. CT scanning of selected samples revealed mineral precipitation, though not soft tissue replication, within the pore spaces of the fine bead, medium bead, and illite replicates; such precipitation, if pervasive enough, may restrict system permeability and thus serve as a further check on oxidant diffusion and decay.

Introduction

Taphonomic decay experiments play crucial roles in deducing the mechanisms behind exceptional fossilization (Behrensmeier and Kidwell, 1985). By studying taphonomic biases in controlled laboratory settings, paleontologists can better identify their presence in the fossil record and thus shed light on how the twin processes of decay and mineralization regulate preservation (Briggs, 1995). Yet while much work has been done on clarifying each of these factors individually, the exact relationship between them remains elusive. While exceptional fossilization requires the inhibition of decay (Allison, 1988; Briggs and Kear, 1994), it also generally necessitates the promotion of authigenic mineralization, which is encouraged by microbial activity (Briggs, 2003). Thus, decay and mineralization are not strictly inverse processes; rather, they are to some extent directly associated, with an initial amount of the former

needed for the latter (Briggs and Kear, 1993a; Sagemann, 1999). The complete elucidation of their interaction will necessitate the refinement of existing experimental models, which will enable the clarification of more specific taphonomic questions (Briggs, 1995). Sediment will almost certainly feature prominently in any such developments, with its consideration as a key taphonomic parameter promising to spur debate on preservational biases previously left unexplored.

Although substrate conditions likely represent an important control on organic preservation (Butterfield, 1995), their experimental modeling is difficult and has generally been avoided by paleontological investigators. Taphonomic experiments typically measure decay through the assessment of the selected organism's morphological decomposition; burial within sediments essentially renders such diagnoses impossible, with experiments that attempt to surmount the difficulties of excavation losing much of their precision (Allison, 1988; Briggs and Kear, 1994). The investigation by Plotnick (1986) of arthropod preservation potential represents perhaps the only taphonomic attempt to describe substrate-based decay using entirely qualitative methods, with the results demonstrating the shortcomings of doing so. Having initially buried shrimp carcasses on an open beach, Plotnick (1986) found himself unable to relocate them for excavation and consequently repeated the experiment in a more controlled laboratory setting, sieving his experimental sediments to model ideal substrate conditions. Unfortunately, his sampling regimen—repeatedly excavating, examining, and then reburying the carcasses over the course of four weeks—hastened disarticulation and rendered his morphological observations suspect. This sort of methodological inability to account for sediment has precluded its full investigation and, as Butterfield (1995) notes, thus implicitly validated its characterization as an “inert packing material” unworthy of study. Overcoming such prejudices will require experimental proof that substrate conditions influence decay, which in turn will necessitate the development of innovative sampling methodologies capable of producing such evidence (Briggs, 1995).

Researchers following Plotnick (1986) have almost uniformly attempted to measure substrate-based decay using quantitative techniques, eschewing his morphological observations for more robust analyses. While these have generally been more successful, Allison's investigations of substrate anoxia (1988; 1990) demonstrate that even quantitative sampling methodologies have sedimentary limitations. Having noted the futility of morphologically

diagnosing excavated carcasses, Allison (1988) chose to measure decay as a function of weight loss by massing discrete tissues before and after burial. Less subjective than traditional techniques, this methodology partially surmounted problems of sediment-related disarticulation and has since been incorporated into both substrate-based and aqueous experiments (Briggs and Kear, 1993b; 1994; Hof and Briggs, 1997; Sagemann et al., 1999). Despite their usefulness, however, weight loss measurements can be biased by osmotic intake (Briggs and Kear, 1994) and authigenic mineralization (Sagemann et al., 1999) of the carcass, both of which can significantly reduce sampling precision. Allison's definitive attempt (1990) to justify the application of weight-loss measurements to substrate-based decay thus met only partial success: variation between his treatment groups was overshadowed by disparities within them, preventing him from fully describing a relationship between substrate and decay. While Allison (1990) accounted for this disappointment by citing the environmental heterogeneity of his outwardly homogenous sediments, it is entirely possible that his methods were compromised by the experimental error inherent to even the most conscientious excavation. Weight-based methods, after all, require the physical handling of the experimental tissue during analysis and are thus by definition invasive. The struggles of Plotnick (1986) demonstrated that substrate sampling can only preserve experimental integrity if conducted remotely; Allison's experiments, though well-designed and executed, ultimately serve to validate this maxim.

In this experiment, we test Allison's (1990) suggestion that variations in substrate permeability control microbial decay through the regulation of oxidant diffusion to buried tissues. Gaines et al. (2005; 2012) would later propose an expanded version of this hypothesis as the central tenet of their model for Burgess Shale-type preservation, arguing that the restricted permeability of such deposits so inhibited bacterial activities that soft tissues survived decay as kerogenized carbon films (Gaines et al., 2008). While this mechanism is theoretically plausible, to our knowledge it has yet to be assessed in an experimental capacity, most likely because investigations of permeability must be conducted in the presence of sediment. In testing a permeability model for decay inhibition and exceptional preservation, then, this experiment seeks to advance the paleontological understanding of substrate-based taphonomy in general, which we do through the exploitation of non-invasive sampling methodologies developed for that purpose. Infrared gas analysis (IRGA) and x-ray computed tomography (CT-scanning) are presented here as effective techniques for assessing substrate-based decay and mineralization,

allowing for its various parameters to be controlled between treatment groups and accurately modeled as potential preservational biases. IRGA sampling in particular opens up new lines of taphonomic investigation, with the results derived from its analyses serving as the foundation for the conclusions drawn from this experiment.

Methods

Experimental Setup

Fresh Atlantic cod (*gadus mortua*) was selected to serve as the experimental decay tissue and was procured from a local fish market. Unpublished pilot projects previously initiated by these investigators had used whiteleg shrimp (*Penaeus vannamei*) as the decay tissue due to its known taphonomic decay sequence (Allison, 1988; Briggs and Kear, 1993a; Briggs and Kear, 1994; Hof and Briggs, 1997; Plotnick, 1986) and concordance with taxa commonly found in Burgess Shale-type deposits (Caron and Jackson, 2008). Given that this experiment avoided morphological diagnoses and did not seek to replicate Burgess Shale-type conditions, however, alternative decay tissues were acceptable. Cod was chosen because its muscle tissue could be precisely divided into numerous identically-sourced tissue cubes, ensuring the standardization of the organic material decayed in the various experimental units.

Substrate conditions were modeled with five different sediments: silica beads of three sizes (fine = 40-90 μm , medium = 90-135 μm , and coarse = 400-600 μm) and kaolinite and illite clays. Five experimental treatment groups were thus established, with each corresponding to one of the experimental sediments. The fine bead, medium bead, kaolinite, and illite groups each contained four individual replicates, with the coarse bead group only containing three due to supply limitations. Thus, nineteen experimental replicates were created in total. In each of these, a 0.2 gram tissue cube was encased between two 8-milliliter layers of sediment, inoculated with a pinch of Long Island Sound mud, and then flooded with an additional 11.5 milliliters of artificial seawater, bringing the total volume of each sample to 27.5 milliliters (see Figure 1 for schematic representation). The 50-milliliter centrifuge tubes containing the experimental replicates were then sealed and incubated at room temperature. The tissue cubes encased within each replicate were massed before burial in order to ensure that they did not vary by more than

twenty percent from the standard mass; after preparation, they remained undisturbed for the duration of the experiment.

In addition to the five experimental treatment groups, one control group was also established. In these replicates, exposed tissue cubes were inundated without sediment in 27.5 milliliters of artificial seawater. Ten such replicates were created, with their masses varying: four contained 0.20 grams of tissue, three 0.10 grams of tissue, and three 0.30 grams of tissue. An eleventh control replicate was prepared with no tissue at all. Like the experimental replicates, the control replicates were sealed after preparation and left undisturbed; the tissue cubes sank to the bottom and remained there for the duration of the experiment.

The artificial seawater used in the experiment was created by mixing 0.5 cups of artificial calcium powder with 1 gallon of deionized water (proportionally, 0.25 cups calcium powder with 0.5 gallons of water, or 59 milliliters calcium powder with 1893 milliliters of water). This mixture was inoculated with 140 milliliters of seawater taken from the Long Wharf beach in New Haven to ensure the presence of bacteria; 30 milliliters of solid calcium chloride pills were also mixed in to encourage mineral precipitation. Supplementary analysis via ion chromatography (IC) and inductively coupled plasma optical emission spectrometry (ICP-OES) revealed that this solution contained no ionic components uncommon to natural seawater (Pilson, 1988; chapter 4).

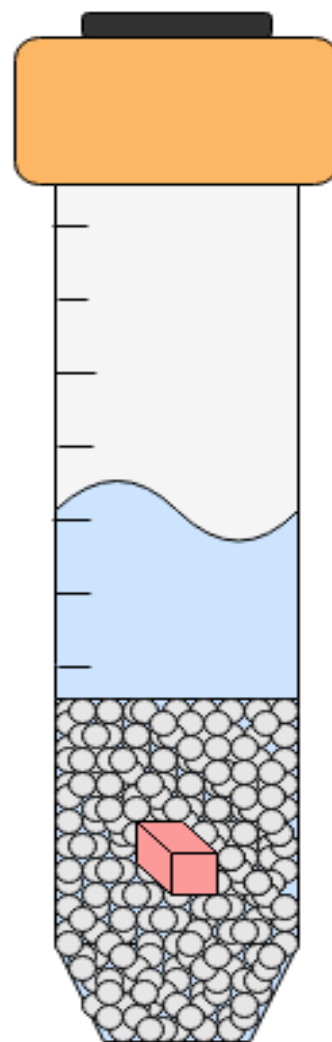


Figure 1. Schematic representation of an individual experimental bead replicate. Not to scale.

Analyses I: Decay Rate Measurements

Infrared gas analysis (IRGA) was used to measure the rate at which carbon dioxide was emitted from each sample. IRGA measures the interference by gas samples on projected infrared wavebands; because carbon dioxide readily absorbs such wavebands, discrepancies between the IRGA beam projector and detector reflect its concentration (Mulkey and Smith, 2008). The

integral values that result can be correlated with a standard gas solution to calculate the parts per million concentration and total flux volume of any carbon dioxide present. The IRGA model used, an LI-7000 CO₂/H₂O analyzer from Li-COR Biosciences, can measure carbon dioxide concentrations to the individual micromole and is therefore a powerful tool for quantifying gas fluctuations within closed environments. While many IRGA-based experiments have studied photosynthetic gas exchange (Long et al., 1996), some have focused on microbial-induced soil respiration (Bekku et al., 1995), a phenomenon similar to the experiments conducted here.

IRGA analysis was conducted over a period of thirty-three days, with Day 1 sampling initiated twenty four hours after sample preparation. Because high carbon dioxide concentrations reduce IRGA accuracy, sampling was performed as often as possible, daily during peak carbon dioxide production and generally at least three times per week. To prevent the buildup of excess carbon dioxide, the centrifuge headspaces were flushed for three minutes with carbon dioxide-free gas following every sampling event. Therefore, carbon dioxide concentrations were interpreted as rates rather than total volumes, standardized as milliliters of carbon dioxide produced per hour per gram of fish. Replicates remained sealed for the duration of IRGA analysis, with invasive sampling not initiated until SEM analysis.

Analyses II: Mineral Precipitation Measurements

Immediately following IRGA sampling, selected replicates were analyzed by x-ray computed tomography (CT-scanning) in order to identify any mineral precipitation that had occurred during decay. One sample from each of the five experimental groups and one sample from the 0.2 gram control group were imaged using an eXplore CT 120 micro-CT scanner from General Electric, which captured image slices at resolutions of 40 micrometers throughout the entirety of each replicate. The resultant frames were used to select promising samples for supplemental analysis by scanning electron microscopy (SEM), which was undertaken with the goal of capturing images of bacterial pitting and authigenic mineralization similar to those produced by Briggs and Kear (1994) and Hof and Briggs (1997).

Structures of interest revealed by SEM were further investigated by energy dispersive x-ray spectroscopy (EDS), which conducted rudimentary diagnoses of elemental presence or absence. Although EDS could not quantitatively measure elemental concentrations, the relative data it provided was used to infer the chemical composition of selected regions. Similar

techniques were previously exploited by Gaines et al. (2005) and Lin et al. (2011) to infer the compositions of mineralized fossil tissues. Unlike CT-scanning, SEM and EDS analysis required the physical excavation and manipulation of the sample sediments, which was carried out by hand with the use of precise picking tools and micrometer-scale sieves.

Results

Results I: Decay Rate Data

Summary

Initial permeabilities of the silica bead replicates were calculated using the Rumpf and Gupte (1975) model, $k = (\epsilon^{5.5}/5.6)d^2$, where k is the permeability, ϵ the porosity, and d the diameter of the spherical particle. Bead porosity was estimated as 0.383, the reference value given by Dullien (1992) for poured, randomly packed spherical particles; grain diameters were averaged to 500 μm for the coarse beads, 112.5 μm for the medium beads, and 65 μm for the fine beads. Thus, the bead permeabilities were estimated as 227.69 μm^2 for the coarse beads, 11.53 μm^2 for the medium beads, and 3.85 μm^2 for the fine beads. As Andersen and Kristensen (1992) demonstrate, sediment porosity can be more exactly calculated by capturing the evaporation of infiltrated water; given the aims of this experiment, however, scientific estimates were sufficient.

Individual replicates within each experimental treatment group emitted similar amounts of carbon dioxide at the same rates and were thus averaged together to produce trendlines indicative of their general decay progressions (complete sampling records can be viewed in Appendix I). The peaked nature of the carbon dioxide emission rates observed in nearly all samples corroborates other charted accounts of quantitatively-measured decay (Allison, 1990; Andersen and Kristensen, 1992) and suggests that, under idealized conditions, organic matter can survive indefinitely. No tissue masses were fully dissipated over the course of the experiment; outside the laboratory, of course, natural processes recycle organic matter on a time scale far quicker than the one here (Plotnick, 1986).

Silica Bead Replicates

The silica bead replicates evidenced two general decay progressions (Figure 2). While the coarse bead samples produced more total carbon dioxide than the medium bead samples, their graphs mirrored each other in slope and peaked simultaneously between Days 14 and 15, at 110

microliters of carbon dioxide per hour per gram of fish each. These results contrasted sharply with the fine bead samples, which produced far less carbon dioxide throughout the course of the experiment and never reached a conclusive emissions peak. The greatest carbon dioxide production rate achieved by the fine bead samples, reached on Day 31, was only 19 microliters of carbon dioxide per hour per gram of fish; given their group's overall emission trend and the cumulative amount of carbon dioxide emitted by the other samples, this value likely represents a localized peak rather than a true maximum in decay.

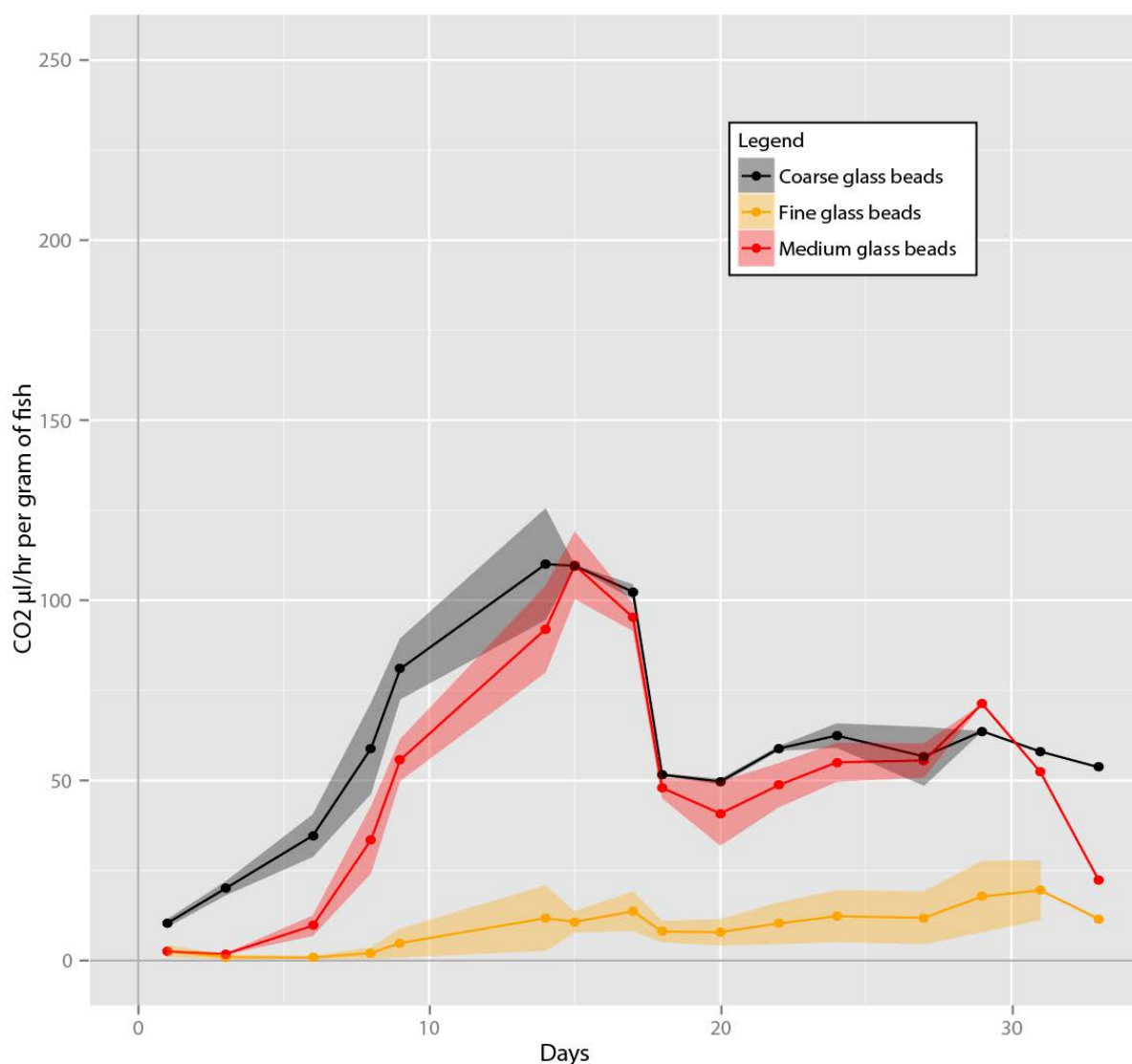


Figure 2. Silica bead carbon dioxide emissions, with decay rates of fine bead, medium bead, and coarse bead samples.

Clay Replicates

In general, the kaolinite samples produced more carbon dioxide than the illite samples, with the discrepancy most pronounced during the first half of the experiment (Figure 3). However, the emissions rates for both clays mirrored each other closely in terms of their general trend. Both groups peaked in production on Day 15, with the kaolinite samples averaging 83 microliters of carbon dioxide per hour per gram of fish and the illite samples averaging 53 microliters per hour per gram of fish.

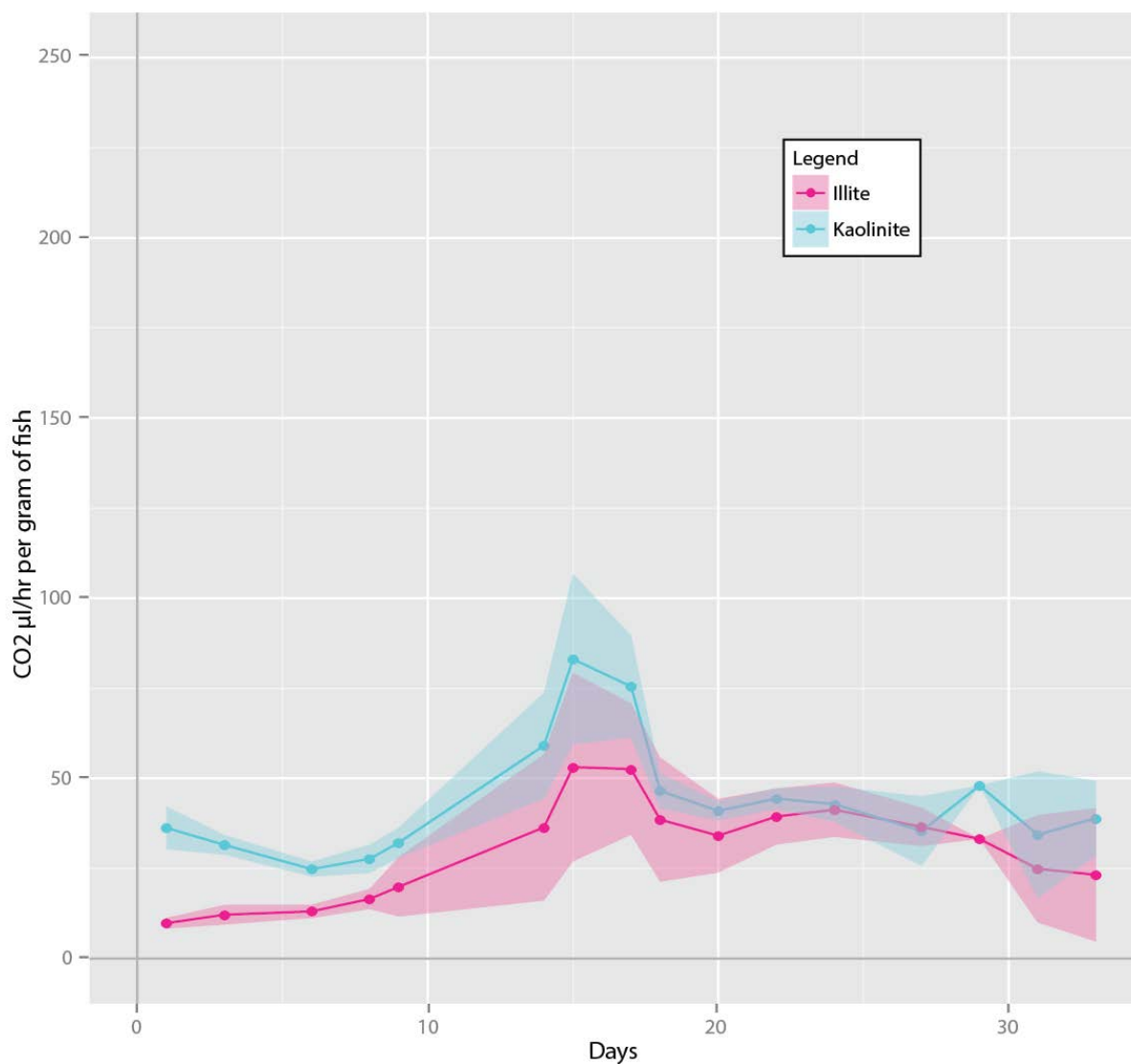


Figure 3. Clay carbon dioxide emissions, with decay rates of illite and kaolinite samples.

Control Replicates

The control samples evidenced differential carbon dioxide emissions based on their masses and were graphed accordingly (Figure 4). The 0.1 and 0.2 gram samples followed each other's emission trends closely, with the 0.1 gram samples producing slightly more carbon dioxide before peak production but the 0.2 gram samples producing more afterwards. Both groups peaked on Day 9, at 216 and 217 microliters of carbon dioxide per hour per gram of fish respectively. In contrast, the 0.3 gram samples peaked on Day 15 at 145 microliters of carbon dioxide per hour per gram of fish. Until this point, its carbon dioxide emission rates had been substantially less than those of the 0.1 and 0.2 gram groups; however, its trendline surpassed their graphs on Day 16 due to its less pronounced post-peak decline. As expected, the control replicate that contained no tissue produced negligible amounts of carbon dioxide compared to the others, and was consequently not graphed.

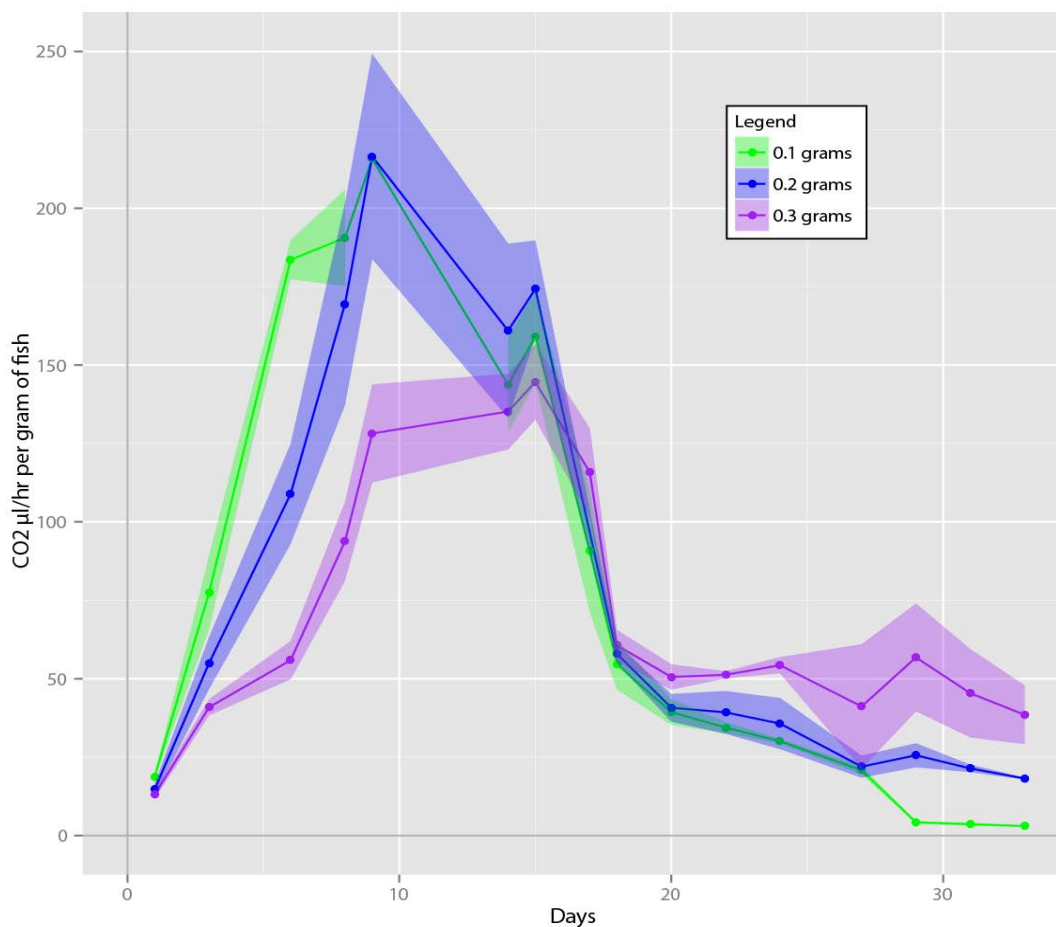


Figure 4. Control carbon dioxide emissions, with decay rates of 0.1, 0.2, and 0.3 gram tissue samples.

Results II: Mineral Precipitation Data

CT-Scanning Evidence of Mineral Precipitation

CT-scan images were defined by a grayscale density gradient in which regions of higher density were shaded lighter in color than regions of lower density. Consequently, empty air pockets appeared darkest, followed by the slightly lighter fish tissue (approximately 1.05 g/cm^3 (Alexander, 1958)) and the various experimental sediments (silica beads approximately 2.5 g/cm^3 according to their manufacturers; kaolinite clay approximately 2.65 g/cm^3 and illite clay approximately 2.75 g/cm^3 (Totten et al., 2002)). The brighter flakes and specks that appeared in some of the samples were of a different hue entirely and were consequently interpreted as evidence of mineral precipitation. Two lines of evidence supported this conclusion. First, the densities of many authigenic minerals commonly produced in decay experiments exceed those of the experimental sediments and would thus have a lighter grayscale shading. Second, authigenic minerals reported in the literature have a size consistent with the high-density regions observed here, which at 40 to 135 micrometers in diameter fell within the general range reported by Briggs and Kear (1994) and Hof and Briggs (1997). SEM imaging would subsequently indicate that the individual mineral crystals present in the samples rarely exceeded lengths of 10 micrometers, suggesting that the high-density regions evidenced by CT-scanning represented hotspots of crystallization rather than specific mineral grains themselves.

CT-scanning did not reveal mineral precipitation in all of the experimental treatment groups. While prevalent in the fine bead, medium bead, and illite samples (Figures 5-7), high-density regions were wholly absent from the coarse bead and kaolinite ones (Figures 8-9), resulting in those samples' being studied more cursorily during SEM analyses. The fish tissue itself was never observed to be mineralized in any of the treatment groups and was consequently excluded from all SEM analyses; instead, clumped and discolored sediments were preferentially excavated due to their potential to represent mineral cementation. The replicates that provided these sediments had been allowed to incubate for roughly 120 days following CT-scanning; it was hoped that this delay would allow for the growth and further proliferation of any precipitated mineral crystals.

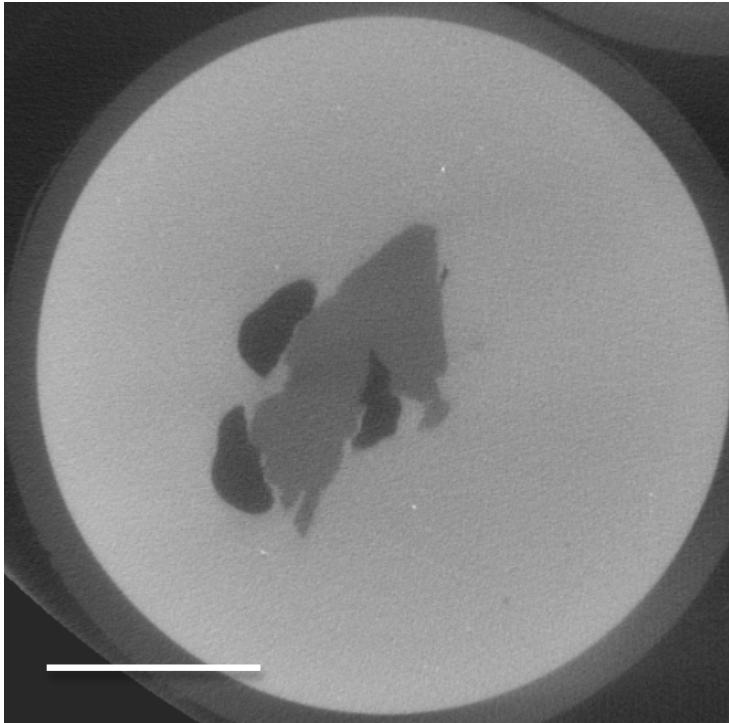


Figure 5. CT-scan of fine bead replicate. Transverse orientation. Scale bar approximately 1 centimeter. Lighter regions of high gravity suggest potential sites of mineral precipitation. Central structure represents fish tissue surrounded by air pockets.

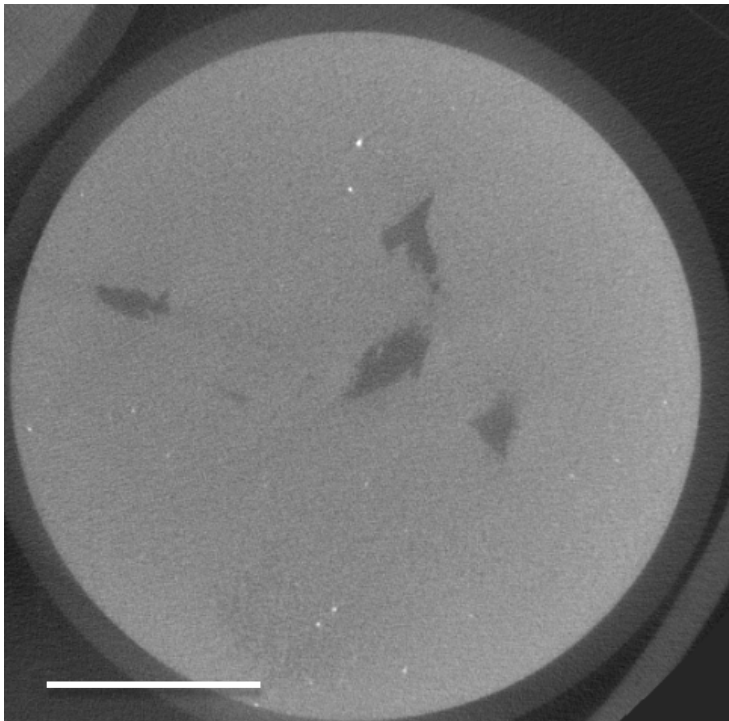


Figure 6. CT-scan of medium bead replicate. Transverse orientation. Scale bar approximately 1 centimeter. Lighter regions of high gravity suggest potential sites of mineral precipitation. Darker regions represent fish tissue.

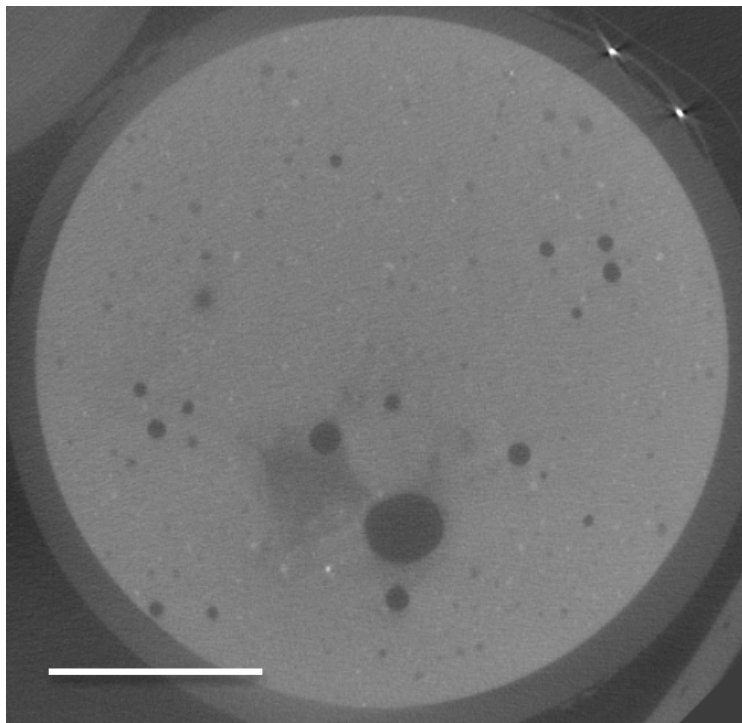


Figure 7. CT-scan of illite replicate. Transverse orientation. Scale bar approximately 1 centimeter. Lighter regions of high gravity suggest potential sites of mineral precipitation. Darker regions alternately represent fish tissue or air pockets.

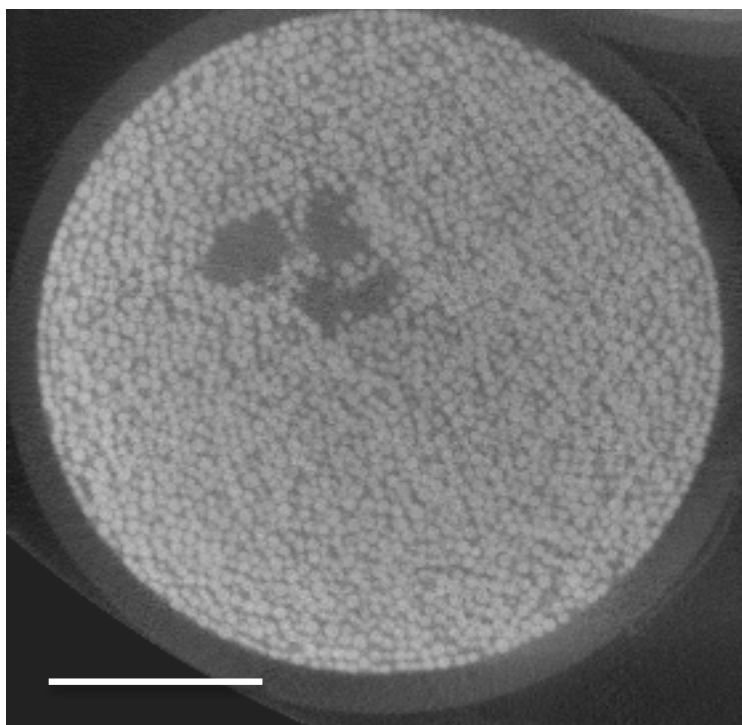


Figure 8. CT-scan of coarse bead replicate. Transverse orientation. Scale bar approximately 1 centimeter. No evidence of mineral precipitation. Darker regions represent fish tissue.

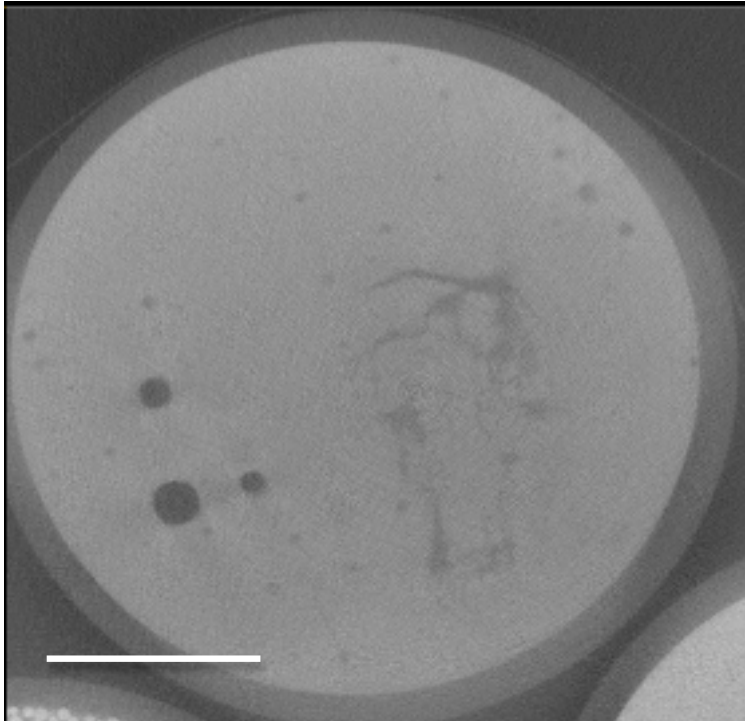


Figure 9. CT-scan of kaolinite replicate. Transverse orientation. Scale bar approximately 1 centimeter. No evidence of mineral precipitation. Darker regions alternately represent fish tissue or air pockets.

SEM and EDS Identification of Mineral Precipitation

Although SEM analysis failed to reveal any mineral precipitation within the illite, kaolinite, or coarse bead samples, numerous mineralized structures were observed throughout the medium and especially fine bead samples. These were classified as representing three different crystal morphologies and were subsequently recognized as carbonate minerals. EDS analysis was helpful in validating mineral identifications but suffered interference from the platinum SEM coating, silica glass beads, and evaporative salts that pervaded the sediments.

The first crystal morphology, mineralized spars normal to or flushed against the bead surfaces (Figure 10), had been previously reported in taphonomic experimentation by Briggs and Kear (1994) and was identified as acicular aragonite. These minerals formed radiating bundles but were also manifested as independent crystal needles whose terminal ends were occasionally squared off rather than pointed (Figure 11), a characteristic described by Flügel (2010; pg. 292) as diagnostic. EDS analysis supported this interpretation by returning peaks for both calcium and oxygen (Figure 12).

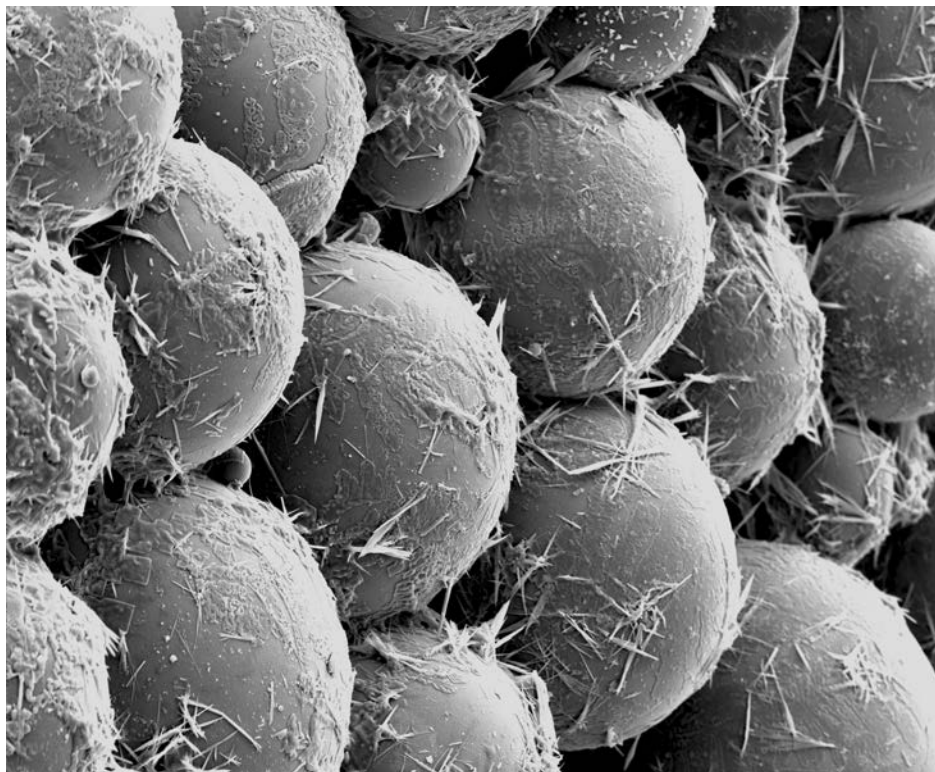


Figure 10. Low resolution SEM image of fine bead sample, with sediment surfaces evidencing pervasive acicular mineral precipitation.



Figure 11. High resolution SEM image of fine bead sample. Acicular mineral precipitation interpreted as aragonite needles and bundles. Central glue-like structure likely represents evaporative salt, as suggested by EDS.

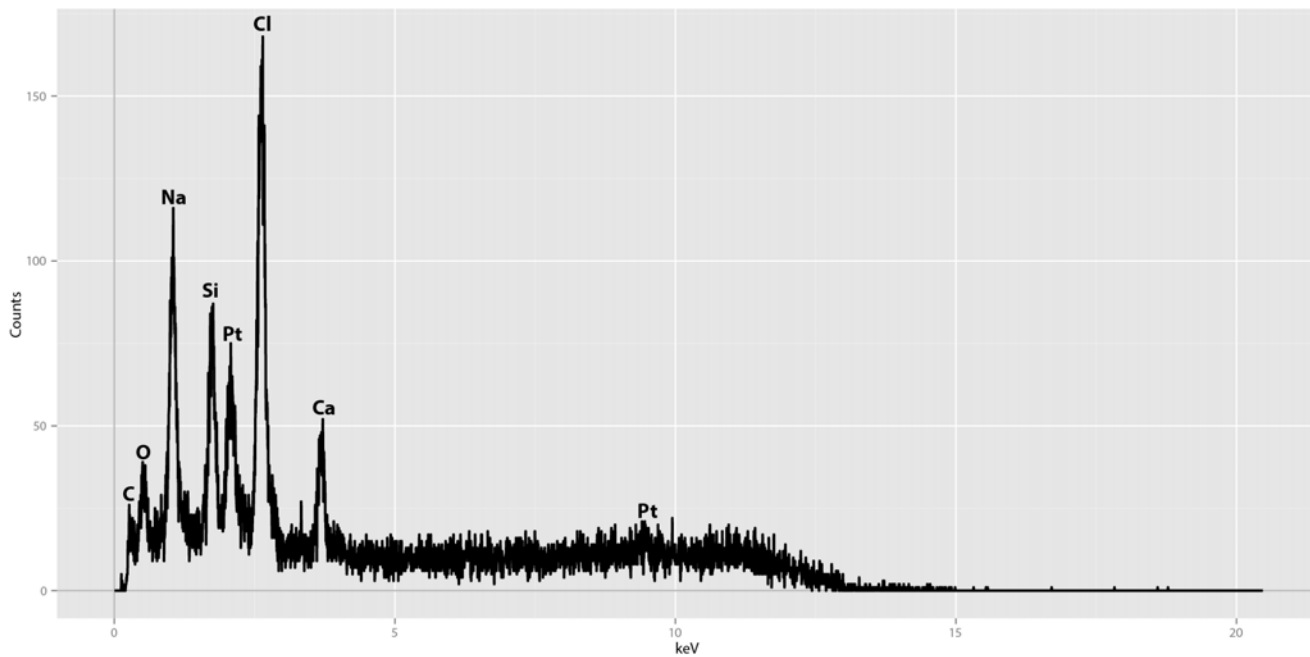


Figure 12. EDS analysis conducted on region imaged in Figure 11. Calcium and oxygen peaks suggest the presence of a carbonate mineral, interpreted as aragonite.

The second crystal morphology, a flat, pitted pavement that coated the bead surfaces (Figure 13), was identified as sheeted calcite. This conclusion was validated by the amorphous crystallization and porous texture of the mineralization, which matched descriptions for calcite bundles previously provided by Briggs and Kear (1994). EDS analysis supported this interpretation by returning peaks for both calcium and oxygen (Figure 14).

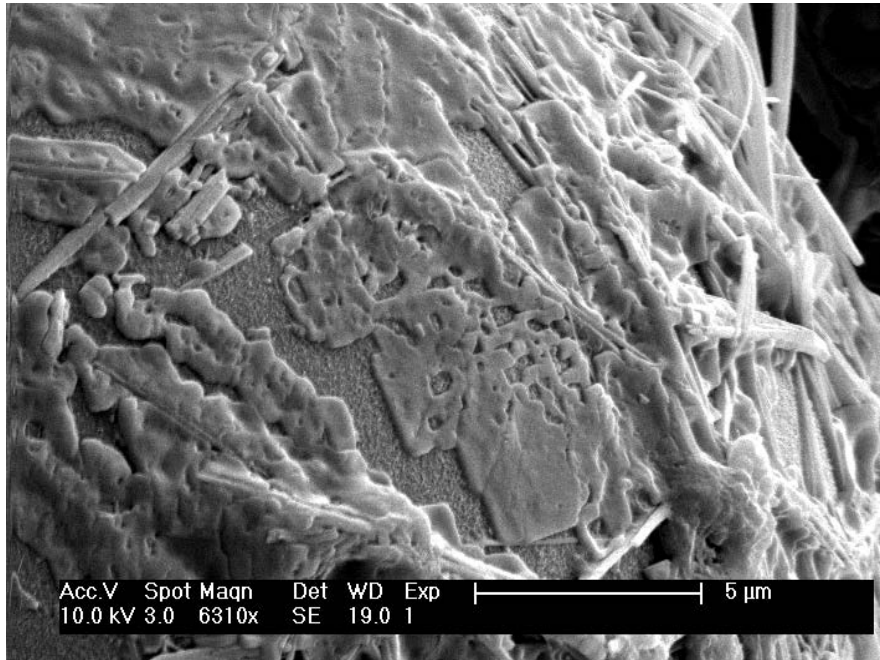


Figure 13. High resolution SEM image of fine bead sample. Pavement-like mineral precipitation interpreted as sheeted calcite.

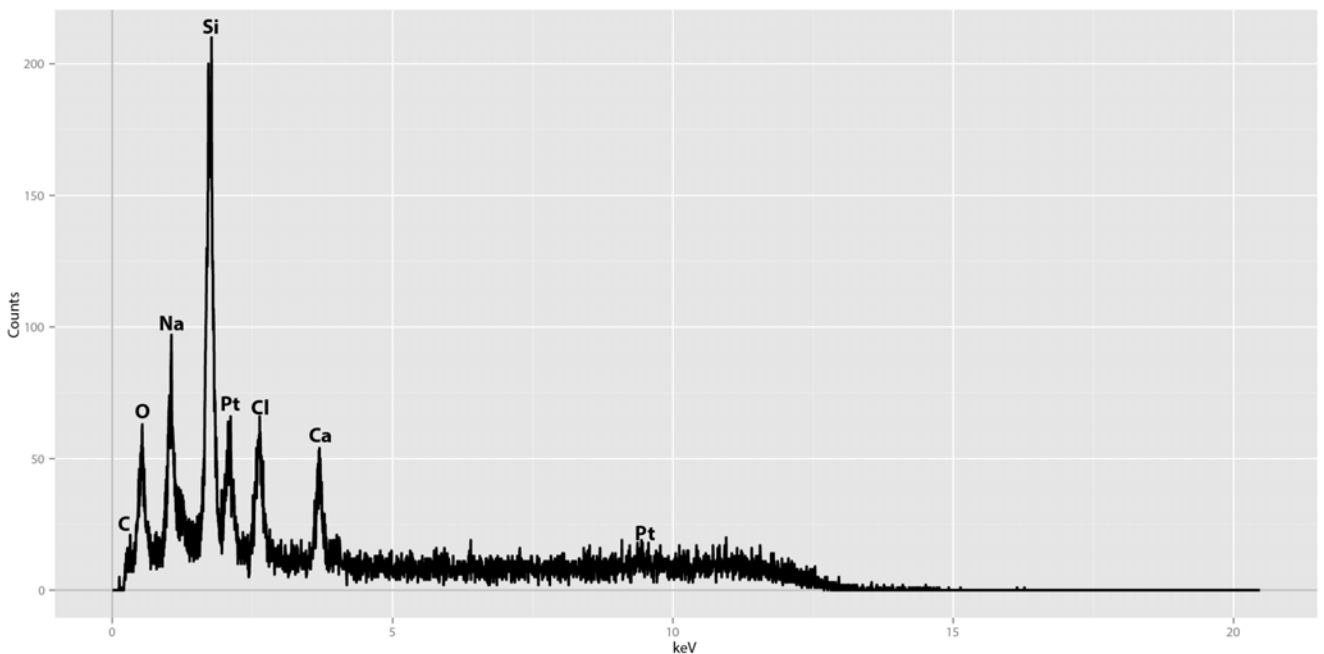


Figure 14. EDS analysis conducted on region imaged in Figure 13. Calcium and oxygen peaks suggest the presence of a carbonate mineral, interpreted as calcite.

The third crystal morphology, a closely packed pavement of stubby crystals with triangular cross-sections (Figures 15-16), compared favorably with the high-magnesium calcite cement described by Flügel (2010; pg. 290-291). EDS analysis conducted on this morphology returned unique magnesium peaks in addition to oxygen and calcium ones (Figure 17), strongly suggesting the validity of the identification.

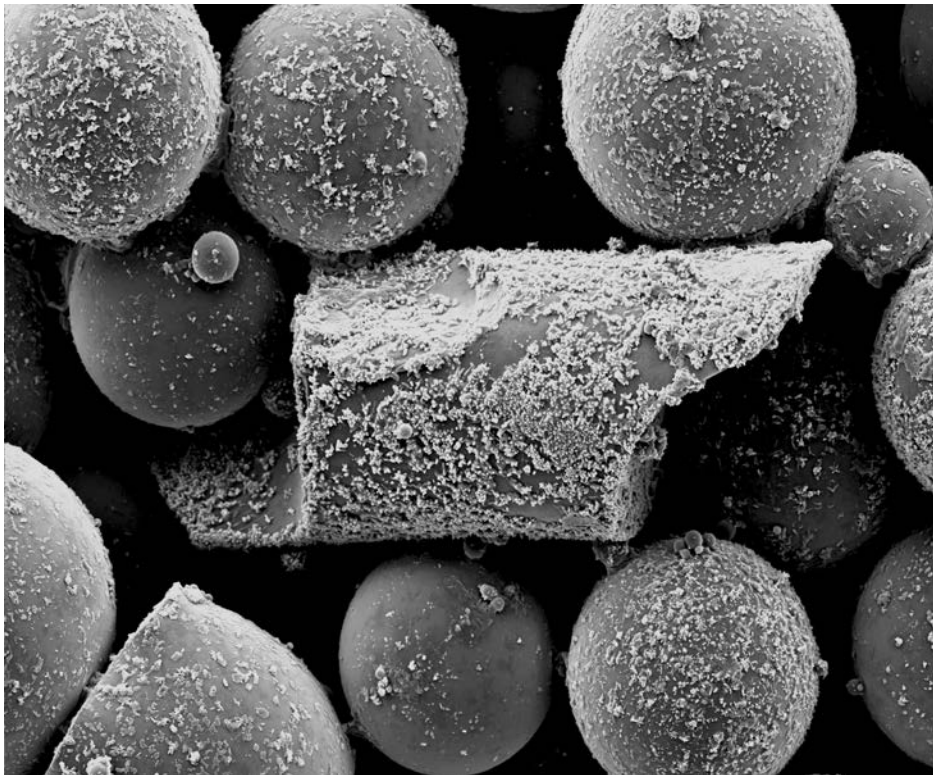


Figure 15. Low resolution SEM image of fine bead sample, with sediment surfaces evidencing pervasive pavement-like mineral precipitation.

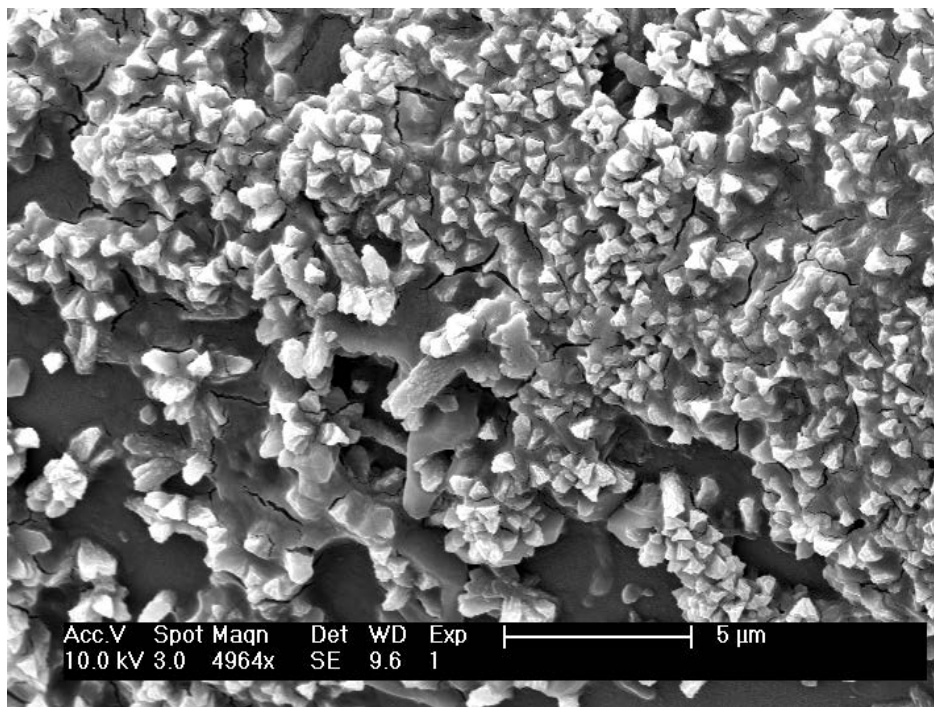


Figure 16. High resolution SEM image of fine bead sample. Dense, trigonally-structured mineral precipitation interpreted as magnesium calcite.

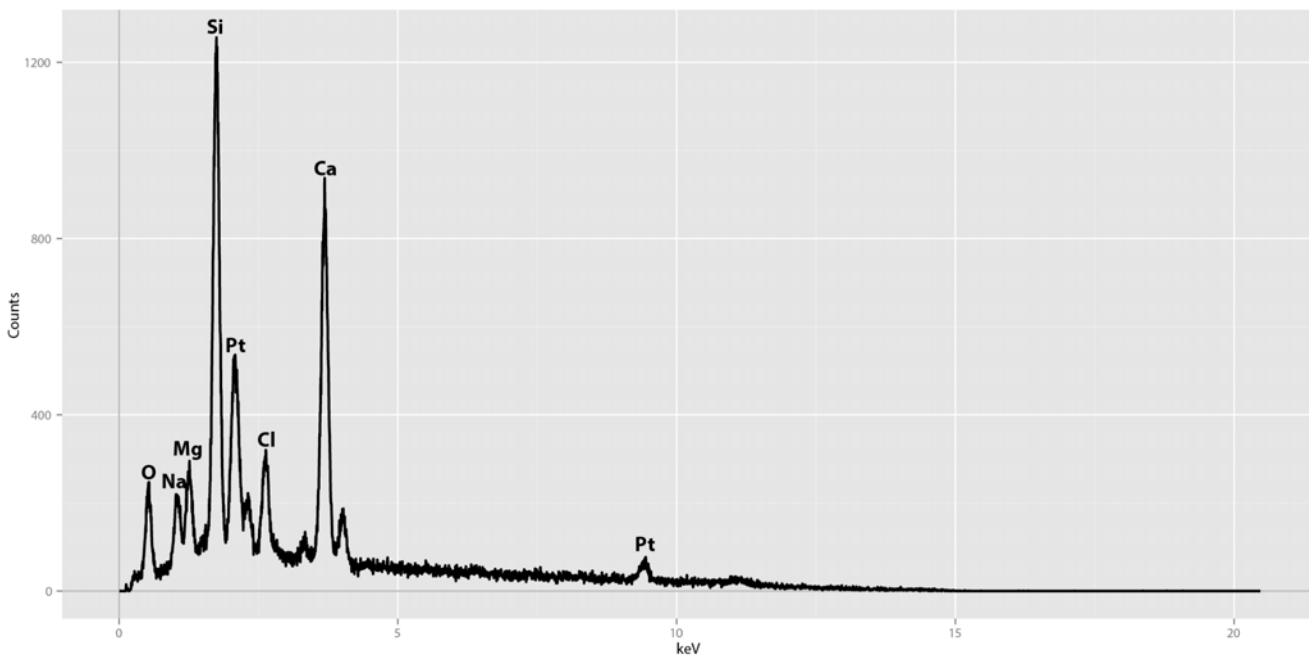


Figure 17. EDS analysis conducted on region imaged in Figure 16. Calcium, oxygen, and magnesium peaks suggest the presence of a carbonate mineral, interpreted as magnesium calcite.

Discussion

Decay and Substrate Permeability

Data derived from this experiment was interpreted with the assumption that the production of carbon dioxide can be used to model decay (as postulated by Andersen and Kristensen (1992) in a more biologically-oriented study). Our control replicates, designed to test this statement, at first glance appear to invalidate it: the heavier tissue masses, expected to undergo the most decay and emit an accordingly proportioned amount of carbon dioxide, were in general outperformed by the lighter ones (Figure 4). This contradiction, however, can be explained by the surface to volume ratios of the cube-shaped tissue masses. Because of their size, the smaller tissues would have been more fully penetrated by bacteria earlier than the larger ones; consequently, they initially emitted more carbon dioxide. By the end of the experiment, bacteria had thoroughly infiltrated all the tissue samples, resulting in the manifestation of the expected carbon dioxide trends. Ultimately, then, the control replicates indicate that carbon dioxide emission rates can indeed be accepted as a relative proxy for decay, legitimizing the conclusions subsequently drawn from IRGA data.

Our experiments validate the hypothesis that permeability and decay are related by a strongly positive association (Gaines et al., 2005; 2012). The relatively impermeable fine bead replicates clearly emitted less carbon dioxide than the medium bead replicates, which in turn emitted less carbon dioxide than the coarse bead replicates (Figure 2). Because all other experimental variables (tissue mass, water composition, bacterial load, sunlight exposure, etc) were standardized across the various experimental treatment groups, this trend indicates the potential of permeability to serve as a major control on the preservation of organic matter (as initially predicted by Allison (1990)). That the control replicates underwent by far the most decay (Figure 4) only further validates this conclusion: with their tissue masses exposed to infinitely permeable conditions, these samples allowed for unrestricted oxidant diffusion and consequently decomposed to the furthest extent.

Despite the overall strength of the IRGA data, the inconsistent correlation between the specific permeabilities and decay rates of the various treatment groups is somewhat problematic. While the fine and medium bead replicates were far closer to each other in permeability than either was to the coarse bead replicates, their carbon dioxide emission rates are surprisingly

divergent, with those of the medium beads mimicking the coarse beads (Figure 2). Partially accounting for this discrepancy is the possibility that some of the carbon dioxide emitted by the fine bead samples remained trapped in the sediment and thus escaped IRGA measurement, as indicated by CT-scan evidence of subterranean air pockets (Figure 5). A more intriguing explanation, however, is that there exists some minimum level of permeability above which oxidant diffusion (and thus decay) proceeds relatively uninhibited. Though ostensibly unlikely, a threshold of this sort would not necessarily need to fall directly between the medium and fine bead permeabilities: in theory, it could lie beneath both of them, with the otherwise disproportional decay inhibition evidenced by the fine bead samples facilitated by mineral precipitation.

Decay and Mineral Precipitation

Decay has long been associated with the precipitation of calcium carbonate and has more recently been recognized as a key controlling factor in its formation (Berner et al., 1970; Chafetz and Buczynski, 1992; Briggs and Kear, 1994). Bacterial decay reactions (see Berner, 1981) initially lower and then subsequently elevate pH levels, resulting in an early buildup of carbonate saturation that subsequently leads to precipitation (Briggs and Kear, 1994; Hof and Briggs, 1997). Mineral cations can be derived either from the environment or from the decaying organism itself, with the magnesium and calcium observed in this experiment perhaps originating in the artificial seawater (Briggs, 2003). That calcium phosphate precipitation was not observed is somewhat surprising, given that fish tissue can provide a steady source of phosphate ions (Briggs and Kear, 1993a). However, Sagemann et al. (1999) reported that calcium phosphate stabilizes at a lower pH than calcium carbonate, suggesting that any precipitation may have been recrystallized as calcium carbonate during the ensuing pH rebound, before sampling occurred. pH meters are commonly applied to taphonomic experiments to monitor changes in sample alkalinity (Briggs and Kear, 1994; Sagemann et al., 1999); their use here, however, would have been invasive and was thus rejected as non-essential.

While numerous taphonomic experiments have induced the mineralization of soft tissue decayed in aqueous conditions (Briggs and Kear, 1993a; 1994; Hof and Briggs, 1997), this experiment is unique in that it evidences how mineral precipitation within the substrate can also affect decay. CT-scanning and SEM analysis of the fine bead replicates evidenced no

mineralization of the decaying tissue itself; rather, mineral precipitation occurred on the surfaces of the silica beads in the surrounding sediment pores. Though these were never fully occluded, the pervasive deposition of carbonate within them (Figures 10-11; 13; 15-16) would likely have increased the tortuosity of the decay microenvironment and thus restricted its permeability, perhaps depressing it below some critical threshold required for efficient oxidant flow. Such a scenario would explain why the fine bead replicates underwent far less decay than the medium bead replicates (Figure 2): though the two treatment groups had similar initial permeabilities, mineral precipitation would have reduced the overall porosity of the fine beads to a greater proportional extent and thus altered their decay progression more significantly. The mechanism for Burgess Shale-type preservation proposed by Gaines et al. (2005; 2012) envisioned similar conditions in which low original porosity was exacerbated by the precipitation of micron-scale cements during the early stages of decay. This experiment thus demonstrates the potential validity of their model and sheds light on factors that may clarify other examples of exceptional preservation, most notably concretions.

Carbonate concretions are formed by the precipitation of carbonate cements around a central nucleus, the decay of which may provide the super-saturation of ions necessary for localized mineralization (Raiswell and Fisher, 2000). McCoy et al. (in press) argue that such mineralization can decrease the permeability of the decay microenvironment and thus restrict oxidant flux, initiating a positive feedback cycle that further inhibits decay and increases localized preservation potential (Figure 18). Viewed in tandem with the carbon dioxide data, the mineral precipitation observed here supports this hypothesis. Three-dimensional reconstructions of the experimental CT-scans evidence that mineralization hotspots (when present in the fine bead, medium bead, and illite replicates, respectively Figures 5-7) surrounded the decaying tissue in all dimensions, developing in both proximal and more distant vicinities (Figure 19). Because the small size of the experimental vessels imposes an artificial boundary on the decay microenvironment, it is difficult to extrapolate how far such mineral precipitation might have extended had it been spatially unchecked. Nonetheless, this globular pattern of mineral precipitation evokes comparison to concretionary growth via pervasive or (depending on the ultimate size of the decay microenvironment) outwardly-radiating concentric growth (Raiswell and Fisher, 2000). True concretions have never been successfully induced in laboratory conditions (Berner, 1968), but most attempts have not incorporated sediment into their

experimental setups. The results presented here indicate that restricted permeability may be a crucial prerequisite for concretionary preservation, with substrate a necessary component of its modeling.

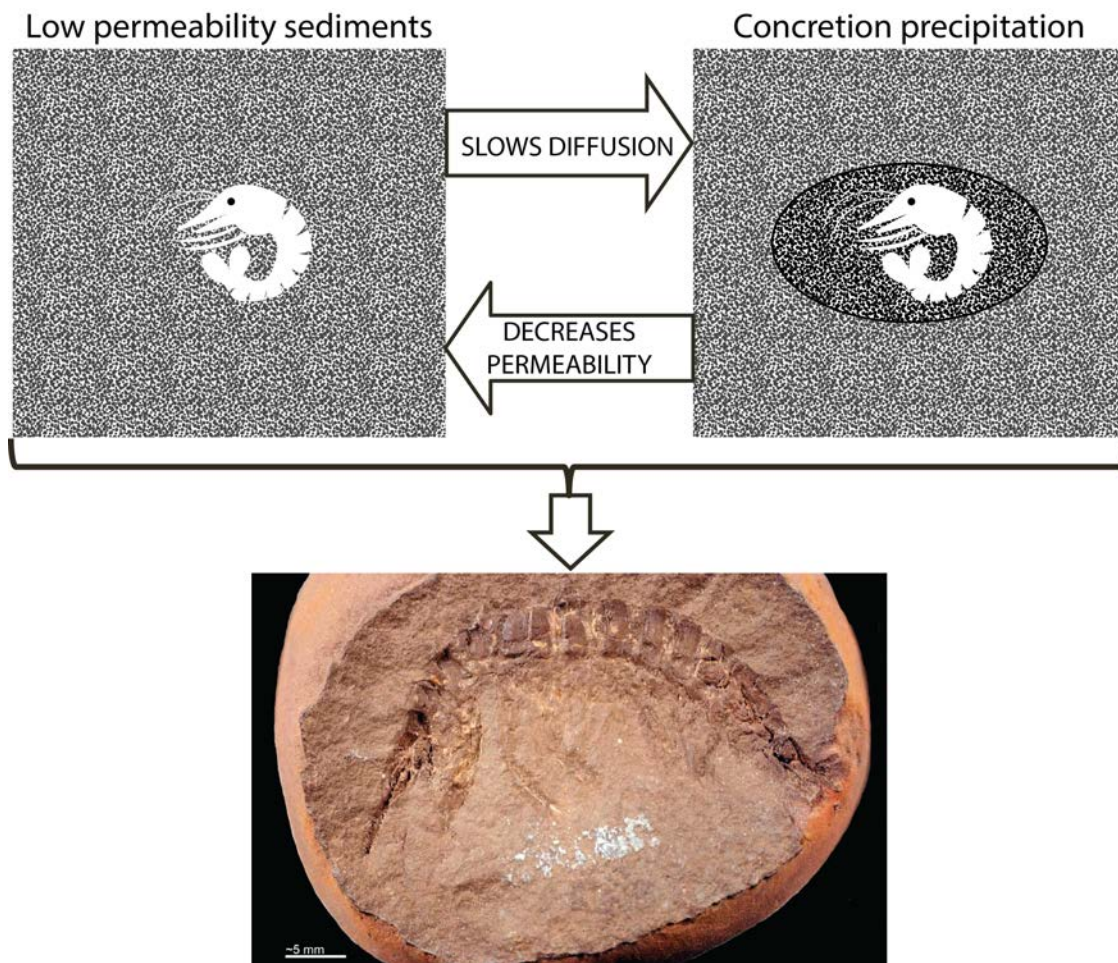


Figure 18. Illustration of positive feedback between sediment permeability and concretionary preservation. Figure from McCoy et al. (in press).

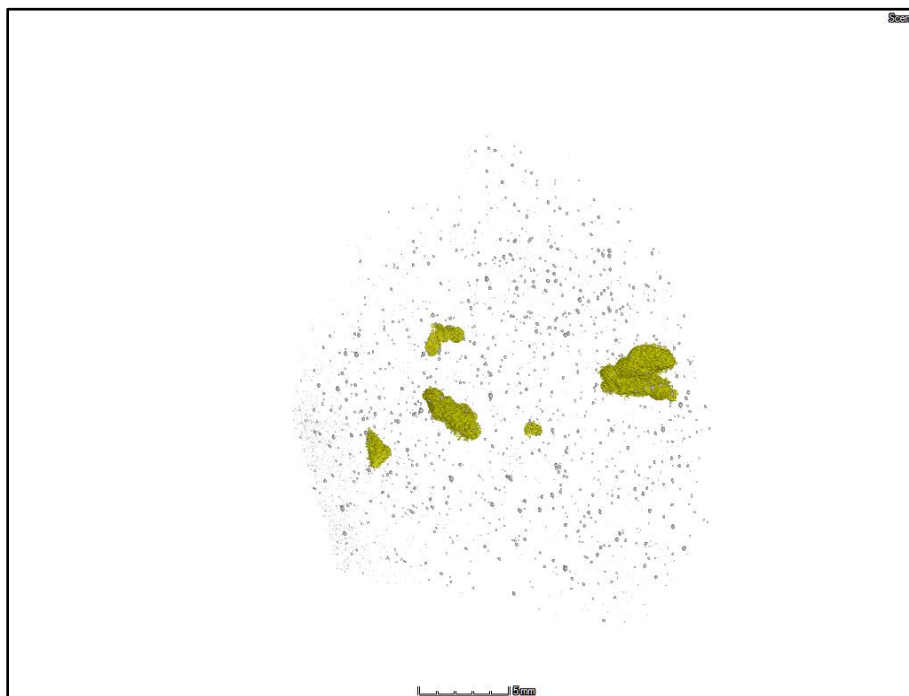


Figure 19. Frame from a video reconstruction of the fine bead CT-scans created using three-dimensional imaging software. Organic tissue depicted in yellow. Scale bar 0.5 centimeters.

Clays

Decay and Substrate Chemistry

Unlike the silica bead replicates, the clay samples could not be controlled so as to only vary in permeability. Their unpredictable grain shapes, bacterial loads, and elemental compositions made them far more heterogeneous than the other experimental treatment groups and thus difficult to compare to them directly. Though their permeabilities were never explicitly measured, clay particles are smaller than even the fine bead replicates, which approximated very fine sand grains (Wentworth, 1922); nonetheless, both the illite and kaolinite replicates produced more carbon dioxide and peaked earlier than them. While the clay carbon dioxide emissions may have been slightly elevated by the presence of organic matter in their dry sediments (as evidenced by auxiliary controls), their decay rates were still greater than would be expected given their assumedly low permeabilities and therefore merited segregation from the silica bead data. Clay treatment groups were introduced to the experiment in order to model substrate chemistry, not permeability; thus, their decay was interpreted independently.

Butterfield (1995) argued that clay minerals contribute to organic preservation by virtue of their cation exchange capacities, which have been proven effective in absorbing and neutralizing degradative enzymes that might otherwise enhance decay (Mortland and Gieseking, 1951; Butterfield, 1990). Clays would therefore be considered an ideal substrate for exceptional preservation, with their presence at numerous Burgess Shale-type deposits corroborating this hypothesis (Butterfield, 1990; Gaines et al., 2008). This experiment investigated the strength of such claims by comparing the decay of organic tissue in illite and kaolinite; both clays have similarly low cation exchange capacities, respectively 10-40 and 3-5 milliequivalents per 100 grams (Carroll, 1959). Mortland and Gieseking (1951) had previously demonstrated illite's greater potential to inhibit specific enzymatic reactions; IRGA analysis validates this trend with regards to decay in general (Figure 3). Though numerous uncontrolled factors likely influenced the clay data, the apparent agreement between these experimental results and the literary representation of clay cation exchange indicates that sediment-organic interactions may indeed play important roles in decay inhibition. If nothing else, the illite-kaolinite dichotomy conclusively disproves the musings of Allison (1990) that compositionally-different substrates might foster essentially similar decay environments. Despite the probable inconsistencies of their respective permeabilities, the illite and kaolinite decay rates were clearly differentiated (Figure 3), indicating that the imprecision of Allison's weight-based measurements likely produced more experimental error than his uncontrolled sediments.

Bacterial Analyses

Visual observations were made on the various replicates during IRGA sampling; these were non-invasive and rather involved diagnosing sediment conditions via the centrifuge tubes' translucent walls. While the silica bead sediments and control sample tissues changed little in appearance, the clay substrates underwent notable color changes throughout the course of the experiment. In several of the illite and kaolinite replicates, the sediment surrounding the decaying tissue had blackened by Day 10, prior to peak carbon dioxide production (Figure 20). Several of the kaolinite samples also developed orange and yellow discolorations that permeated the sediment-water interface and clogged the water column itself (Figure 21). Though the blackened sediment can likely be attributed to anoxia (Allison, 1988), these results were sufficiently intriguing as to merit invasive investigation, which was conducted simultaneously with SEM preparation. Bacterial DNA was extracted from the water columns and sediments of a

single illite and kaolinite replicate; DNA was also extracted from a dry sample of each clay for control purposes. These samples were analyzed by an outside laboratory, which performed microbial diversity analyses on them using tagged pyrosequencing. The data returned percentage and abundance counts for all six samples, revealing their bacterial diversities from the kingdom to species levels.

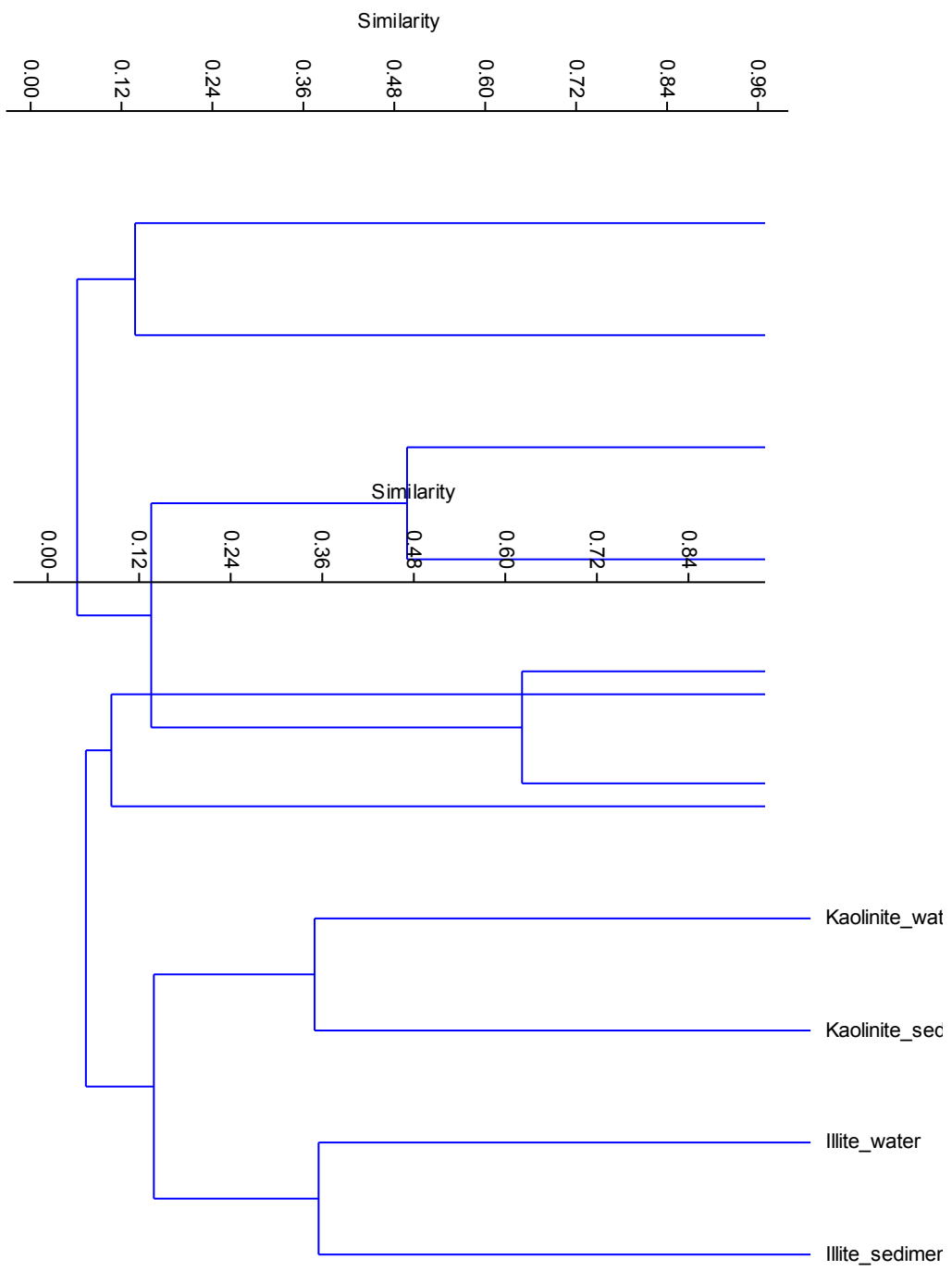


Figure 20. Illite replicate with blackened decay microenvironment.

Preliminary analysis of the microbial data was conducted at the order level for purposes of expediency. Sixty-two bacterial orders were identified in the various samples; however, nine of these composed more than seventy percent of the diversity present in each individual sample (Appendix II). The Bray-Curtis dissimilarity (Figure 22) and Jaccard Index (Figure 23) tests were applied to the entire dataset in order to identify any cluster patterns present; both found concordances between water and sediment samples taken from the same experimental replicate, with the dry control samples identified as closer to each other than either was to its experimental counterpart. This information demonstrates that different clay sediments— even those with similar

initial bacterial loads– foster different bacterial communities, which presumably reflect unique decay microenvironments and sediment chemistries (Butterfield, 1995). Future analyses will more fully explore the significance of this data, which has the potential to unite both taphonomic and bioenvironmental research.

ment



Conclusion

Having quantitatively assessed substrate-based decay in a controlled laboratory setting, this experiment endorses the permeability model for exceptional preservation proposed by Gaines et al. (2005; 2012) and furthermore suggests that sediment chemistry may play a supplementary role in decay inhibition (Butterfield, 1995). The data presented here also helps clarify the “critical balance” between decay and mineralization (Briggs and Kear, 1993a) by indicating that substrate conditions may regulate both. IRGA data evidences that organic decay is at least partially controlled by substrate permeability, but also suggests that permeability itself may be influenced by decay-induced mineral precipitation. A more complete understanding of this relationship will likely require analyses of mineralization more quantitative than the ones performed here, which were limited to presence/absence-type investigations and distributional interpretations. Correlating experimental decay with real-time fluctuations in substrate porosity and permeability would be useful and perhaps possible with the continued development of non-invasive scanning technology. Advances in sampling will thus prove crucial as taphonomic models increase in complexity through the incorporation of sediment and other unexplored variables.

To the best of our knowledge, this experiment represents what may be the most conclusive attempt (rivaled only by Allison (1990)) to characterize substrate-based decay using actualistic methodologies. In providing a permeability-based legitimization for Butterfield’s (1995) general assertion that substrate inhibits decay, its findings have significant ramifications for taphonomic experimentation in general. Unpublished pilot projects previously initiated by these investigators revealed that shrimp carcasses decayed in aqueous systems underwent a different morphological progression than those buried in substrate: the water samples evidenced

Figure 24. Shrimp sedimentary ones previously decayed in aqueous conditions maintained overall integrity but underwent more drastic color change, bloating, and rupturing.

more bloating and rupturing but remained intact far longer than the sedimentary ones previously decayed in aqueous conditions (Figures 24-25). Plotnick (1986) interpreted similar results as proof that sediment expedited decay while water prolonged structural integrity. IRGA analysis indicates the opposite, insinuating that aqueous systems may actually obscure rather than elucidate certain aspects of morphological taphonomy. While aqueous setups are convenient for the modeling of preservational biases (of which permeability is just one), their use in the delimitation of taphonomic thresholds specific to individual taxa may inadvertently produce experimental artifacts rather than true representations of natural decay (as noted by Briggs and Kear (1993b)). Laboratory results must be applied to the fossil record with great care; the data presented here underscores the need to recognize experimental parameters as simplified and interpret their results accordingly (Allison, 1990).





Figure 25. Shrimp previously decayed in sediment underwent disarticulation and fragmentation but retained a more life-like appearance.

Substrate conditions aside, this experiment demonstrates the potential of IRGA for future taphonomic application, either as a supplement to more established methodologies or as a primary analysis on its own. Less subjective than morphological diagnosis and more robust than weight-based measurement, IRGA is most importantly non-invasive, with its analyses supporting the repeated sampling of individual replicates yet still preserving experimental integrity. Furthermore, IRGA sampling is straightforward and easy to conduct, allowing for the rapid testing of numerous samples and thus increasing the statistical power of experiments while minimizing human error. IRGA does have shortcomings; most notably, it cannot distinguish experimentally relevant carbon dioxide from that emitted by more extraneous processes (in this experiment, the decomposition of organic matter likely embedded within the unsterilized clays). Thus, IRGA is probably best employed as a relative rather than absolute measure of decay, with the use of controls ensuring its accuracy. Nonetheless, its relevancy to the measurement of sediment-based decay would appear to be unparalleled. The rise of non-invasive sampling methodologies has the potential to change the way paleontologists think about (or at least

measure) decay– and as this experiment demonstrates, their results can elucidate both sediment-based experimentation and taphonomic investigation in general.

Acknowledgements

Funding for this project was provided by research grants from the Geological Society of America (GSA) and the Paleontological Society. Travel arrangements for the presentation of these results at the GSA Annual Meeting in Denver were jointly covered by a GSA travel grant and the Saybrook College Babcock Travel Research Fellowship. Thanks are due to all for their generosity and commitment to undergraduate research.

While this project was conceptualized within the Derek Briggs laboratory, numerous other researchers provided material and human support crucial for its realization. Most notably, the Mark Bradford laboratory provided IRGA access and training, with Emily Oldfield guiding us through the sampling process. Dr. Zhen Zhuang kindly facilitated the use of a CT-scanner at the Yale Medical School, which was supplemented by work performed in the Gerald Conlogue laboratory at Quinnipiac University. Dr. Ruth Blake and Dr. Jordan Peccia offered consulting on bacterial investigation, with the latter assisting us in DNA extraction. Bacterial analysis was conducted by the Research and Testing Laboratory (Lubbock, Texas), facilitated by Dr. John Hanson. Thanks are also due to Dr. Zhenting Jiang for assisting us with SEM analysis, Dr. Susan

Butts for managing our logistical expenditures, Rachel Racicot for modeling our CT-scan reconstructions, and Dr. Pincelli Hull for offering advice on sampling and serving as the second reader for this paper. Additionally, I would like to convey my appreciation to the Yale University Department of Geology and Geophysics, which has consistently supported my work on this project and offered me a community through which to focus my intellectual development.

As a final note, my two collaborators on this project merit especial mention. I am deeply grateful to my advisor, Professor Derek Briggs, for welcoming me into his laboratory ever since I joined it in 2012 as a summer research assistant. His mentorship has provided me with a wealth of paleontological knowledge and has played a major role in shaping the direction of this project. Above all, I am indebted to Victoria McCoy, who has served as my lab partner and scientific mentor ever since we initiated our first decay experiments last fall. By giving me the chance to participate in her research, Tory has allowed me to gain first-hand experience with the scientific method, shaping my Yale education as much as any of my professors. This project would not have taken place without her expertise, and I am proud to consider myself her “first student.”

Literature Cited

- Alexander, R. M. 1959. The densities of Cyprinidae. *The Journal of Experimental Biology* 36:333-340.
- Allison, P. A. 1988. The role of anoxia in the decay and mineralization of proteinaceous macrofossils. *Paleobiology* 14:139-154.
- . 1990. Variations in rates of decay and disarticulation of Echinodermata: implications for the application of actualistic data. *Palaios* 5:432-440.
- Andersen, F. O. and E. Kristensen. 1992. The importance of benthic macrofauna in decomposition of microalgae in a coastal marine sediment. *Limnology and Oceanography* 37:1392-1403.
- Behrensmeyer, A. K. and S. M. Kidwell. 1985. Taphonomy's contributions to paleobiology. *Paleobiology* 11:105-119.
- Bekku, Y., H. Koizumi, T. Nakadai, and H. Iwaki. 1995. Measurement of soil respiration using closed chamber method: an IRGA technique. *Ecological Research* 10:369-373.
- Berner, R. A. 1968. Calcium carbonate concretions formed by the decomposition of organic matter. *Science* 159:195-197.
- . 1981. Authigenic mineral formation resulting from organic matter decomposition in modern sediments. *Fortschritte der Mineralogie* 59:117-135.
- Berner, R. A., M. R. Scott, and C. Thomlinson. 1970. Carbonate alkalinity in the pore waters of anoxic marine sediments. *Limnology and Oceanography* 15:544-549.
- Briggs, D. E. G. 1995. Experimental taphonomy. *Palaios* 10:539-550.
- . 2003. The role of decay and mineralization in the preservation of soft-bodied fossils. *Annual Review of Earth and Planetary Sciences* 31:275-301.
- Briggs, D. E. G. and A. J. Kear. 1993a. Fossilization of soft tissue in the laboratory. *Science* 259:1439-1442.
- . 1993b. Decay and preservation of polychaetes: taphonomic thresholds in soft-bodied organisms. *Paleobiology* 19:107-135.
- . 1994. Decay and mineralization of shrimps. *Palaios* 9:431-456.
- Butterfield, N. J. 1990. Organic preservation of non-mineralizing organisms and the taphonomy of the Burgess Shale. *Paleobiology* 16:272-286.

———. 1995. Secular distribution of Burgess-Shale-type preservation. *Lethaia* 28:1-13.

Caron, J. B. and D. A. Jackson. 2008. Paleoecology of the greater phyllopod bed community, Burgess Shale. *Palaeogeography, Palaeoclimatology, Palaeoecology* 258:222-256.

Carroll, D. 1959. Ion exchange in clays and other minerals. *Geological Society of America Bulletin* 70:749-779.

Chafetz, H. S. and C. Buczynski. 1992. Bacterially induced lithification of microbial mats. *Palaios* 7:277-293.

Dullien, F. A. L. 1992. Porous media: fluid transport and pore structure. Academic Press Inc.

Flügel, E. 2010. Microfacies of carbonate rocks: analysis, interpretation and application, 2d ed. Springer Publishing Company.

Gaines, R. R., D. E. G. Briggs, and Z. Yuanlong. 2008. Cambrian Burgess Shale-type deposits share a common mode of fossilization. *Geology* 36:755-758.

Gaines, R. R., E. U. Hammarlund, X. Hou, C. Qi, S. E. Gabbott, Y. Zhao, J. Peng, and D. E. Canfield. 2012. Mechanism for Burgess Shale-type preservation. *Proceedings of the National Academy of Science* 109:5180-5184.

Gaines, R. R., M. J. Kennedy, and M. L. Droser. 2005. A new hypothesis for organic preservation of Burgess Shale taxa in the Middle Cambrian Wheeler Formation, House Range, Utah. *Palaeogeography, Palaeoclimatology, Palaeoecology* 220:193-205.

Hof, C. H. J. and D. E. G. Briggs. 1997. Decay and mineralization of mantis shrimps (Stomatopoda: Crustacea)— a key to their fossil record. *Palaios* 12:420-438.

Lin, J. P., A. Y. Ivantsov, and D. E. G. Briggs. 2011. The cuticle of the enigmatic arthropod *Phytophilaspis* and biomineralization in Cambrian arthropods. *Lethaia* 44:344-349.

Long, S. P., P. K. Farage, and R. L. Garcia. 1996. Measurement of leaf and canopy photosynthetic CO₂ exchange in the field. *Journal of Experimental Botany* 47:1629-1642.

McCoy, V. E., R. T. Young, and D. E. G. Briggs. Factors controlling exceptional preservation in concretions. In press.

Mortland, M. M. and J. E. Gieseking. 1952. The influence of clay minerals on the enzymatic hydrolysis of organic phosphorus compounds. *Soil Science Society of America Journal* 16:10-13.

Mulkey, S. S. and M. Smith. 1996. Measurement of photosynthesis by infra-red gas analysis. Pp. 79-84 in J. H. Wandersee, C. T. Lange, and D. R. Wissing. *Bioinstrumentation: tools for understanding life*. National Association of Biology Teachers.

Pilson, M. E. Q. 1998. An introduction to the chemistry of the sea. Prentice Hall Publishing Company.

Plotnick, R. E. 1986. Taphonomy of a modern shrimp: implications for the arthropod fossil record. *Palaios* 1:286-293.

Raiswell, R. and Q. J. Fisher. 2000. Mudrock-hosted carbonate concretions: a review of growth mechanisms and their influence on chemical and isotopic composition. *Journal of the Geological Society* 157:239-251.

Rumpf, H. and A. R. Gupte. 1975. The influence of porosity and grain size distribution on the permeability equation of porous flow. *Chemie Ingenieur Technik* 43:367-375.

Sagemann, J., S. J. Bale, D. E. G. Briggs, and R. J. Parkes. 1999. Controls on the formation of authigenic minerals in association with decaying organic matter: an experimental approach. *Geochimica et Cosmochimica Acta* 63:1083-1095.

Totten, M. W., M. A. Hanan, D. Knight, and J. Borges. 2002. Characteristics of mixed-layer smectite/illite density separates during burial diagenesis. *American Mineralogist* 87:1571-1579.

Wentworth, C. K. 1922. A scale of grade and class terms for clastic sediments. *The Journal of Geology* 30:377-392.

Appendix I: IRGA Data Sheets

All values represent milliliters of carbon dioxide produced per hour per gram of fish.

Silica Bead Replicates

Minimum	Mean	Maximum	Variable	Day
0.947370216	2.619779102	4.292187988	Fine	1
0.337578788	0.961037357	1.584495926	Fine	3
0.41311496	0.803007169	1.192899379	Fine	6
0.527148471	2.096764805	3.66638114	Fine	8
0.845345065	4.832876601	8.820408136	Fine	9
2.696692376	11.76043447	20.82417657	Fine	14
7.770630167	10.71094852	13.65126687	Fine	15
8.216719508	13.66711929	19.11751907	Fine	17
5.058989114	8.019877128	10.98076514	Fine	18
4.240624607	7.858459648	11.47629469	Fine	20
4.523234265	10.28890882	16.05458338	Fine	22
5.118478626	12.28660979	19.45474094	Fine	24
4.529212386	11.85724173	19.18527108	Fine	27
7.914041082	17.76441615	27.61479121	Fine	29
11.19526034	19.47692853	27.75859673	Fine	31
0.262724917	11.55635708	23.37543907	Fine	33
2.21513148	2.491164371	2.767197263	Medium	1
1.6762102	1.795463717	1.914717234	Medium	3
6.844156472	9.674275781	12.50439509	Medium	6
24.23573977	33.50985531	42.78397085	Medium	8
49.8686744	55.65618099	61.44368759	Medium	9
80.0304962	92.02377727	104.0170583	Medium	14
100.364102	109.7122311	119.0603603	Medium	15
91.47790011	95.26326712	99.04863412	Medium	17
45.06412827	47.92593426	50.78774026	Medium	18
31.90406598	40.78697285	49.66987972	Medium	20
42.52689154	48.64965604	54.77242055	Medium	22
49.61546343	55.01566469	60.41586595	Medium	24
50.82683079	55.54178738	60.25674397	Medium	27
71.24515718	71.24515718	71.24515718	Medium	29
52.29729981	52.29729981	52.29729981	Medium	31
6.027305906	22.31499756	50.65730103	Medium	33
9.26425688	10.35851233	11.45276778	Coarse	1
18.10150724	20.01465184	21.92779645	Coarse	3
28.79683814	34.66314852	40.5294589	Coarse	6
46.28678541	58.90743999	71.52809458	Coarse	8
72.5020679	80.94782456	89.39358122	Coarse	9
94.56810538	110.0427603	125.5174152	Coarse	14
109.3618208	109.560956	109.7600913	Coarse	15
100.2997358	102.3501398	104.4005438	Coarse	17
51.24454725	51.59726375	51.94998025	Coarse	18

48.92882657	49.67375432	50.41868208	Coarse	20
58.19890923	58.8261947	59.45348017	Coarse	22
59.09513616	62.45295972	65.81078328	Coarse	24
48.52557938	56.66483256	64.80408575	Coarse	27
63.64434342	63.64434342	63.64434342	Coarse	29
57.98991437	57.98991437	57.98991437	Coarse	31
53.65760608	53.65760608	53.65760608	Coarse	33

Clay Replicates

Minimum	Mean	Maximum	Variable	Day	
8.312479957	9.80150804	11.29053612	Illite		1
9.447571562	12.16515478	14.882738	Illite		3
11.23704432	13.08134323	14.92564213	Illite		6
13.74601759	16.52944898	19.31288036	Illite		8
11.6627048	19.90804336	28.15338191	Illite		9
16.07978583	36.40130155	56.72281727	Illite		14
26.96796493	53.12726092	79.28655692	Illite		15
34.36226276	52.57129727	70.78033177	Illite		17
21.31447587	38.54215704	55.76983821	Illite		18
23.87055786	34.08945545	44.30835304	Illite		20
31.641164	39.39809534	47.15502668	Illite		22
33.75620525	41.29462782	48.83305039	Illite		24
31.23976968	36.53731285	41.83485603	Illite		27
33.18130321	33.18130321	33.18130321	Illite		29
10.00492166	24.89759872	39.79027577	Illite		31
4.737997113	23.235323	41.73264889	Illite		33
30.37462625	36.25382407	42.13302189	Kaolinite		1
28.79531861	31.53739437	34.27947014	Kaolinite		3
22.73863419	24.81370013	26.88876608	Kaolinite		6
23.73198243	27.66513095	31.59827948	Kaolinite		8
27.97142822	32.15227744	36.33312666	Kaolinite		9
44.44451413	59.11168688	73.77885962	Kaolinite		14
59.46055278	83.0857272	106.7109016	Kaolinite		15
61.35541793	75.48128102	89.60714411	Kaolinite		17
41.74588608	46.52245496	51.29902384	Kaolinite		18
38.34408383	40.97957221	43.61506058	Kaolinite		20
41.49584013	44.3875292	47.27921827	Kaolinite		22
37.98786361	42.84345543	47.69904726	Kaolinite		24
25.71726149	35.37212586	45.02699023	Kaolinite		27
47.99965614	47.99965614	47.99965614	Kaolinite		29
16.76601276	34.34596795	51.92592315	Kaolinite		31
28.57671582	38.95220546	49.3276951	Kaolinite		33

Control Replicates

Minimum	Mean	Maximum	Variable	Day	
18.06475266	18.78853202	19.51231138	0.1 grams		1
65.73531924	77.42628302	89.11724679	0.1 grams		3
177.361046	183.5583041	189.7555622	0.1 grams		6

175.2683139	190.5800329	205.8917518	0.1 grams	8
175.7079029	215.7442768	255.7806508	0.1 grams	9
128.7100838	143.7662319	158.82238	0.1 grams	14
144.2875376	158.9934696	173.6994015	0.1 grams	15
71.39506001	90.66850098	109.9419419	0.1 grams	17
46.61063215	54.55961063	62.50858911	0.1 grams	18
35.3052673	39.36928171	43.43329611	0.1 grams	20
32.63000959	34.41447171	36.19893383	0.1 grams	22
29.39495442	30.07067058	30.74638673	0.1 grams	24
19.51351566	20.81225994	22.11100421	0.1 grams	27
3.867804963	4.221366111	4.574927259	0.1 grams	29
3.154039447	3.610734111	4.067428776	0.1 grams	31
2.902483699	3.026309279	3.150134859	0.1 grams	33
12.91821342	14.69472614	16.47123887	0.2 grams	1
46.71281865	54.93242139	63.15202414	0.2 grams	3
93.00407728	108.8956084	124.7871394	0.2 grams	6
137.3151019	169.444793	201.574484	0.2 grams	8
183.8538137	216.5173001	249.1807865	0.2 grams	9
133.2100039	160.944949	188.6798941	0.2 grams	14
158.8433389	174.2676547	189.6919705	0.2 grams	15
54.99214072	57.96760597	60.94307122	0.2 grams	18
36.34751708	40.75181951	45.15612195	0.2 grams	20
32.46963542	39.27146551	46.0732956	0.2 grams	22
27.56976348	35.70140967	43.83305586	0.2 grams	24
18.4608584	21.97221013	25.48356186	0.2 grams	27
21.78168882	25.59433122	29.40697362	0.2 grams	29
20.22698966	21.39894567	22.57090167	0.2 grams	31
17.87834306	18.17821717	18.47809128	0.2 grams	33
11.77133649	13.07194442	14.37255235	0.3 grams	1
38.32554389	40.88251208	43.43948027	0.3 grams	3
49.84511123	55.90622494	61.96733864	0.3 grams	6
81.22417092	93.78082175	106.3374726	0.3 grams	8
112.5495982	128.1858563	143.8221144	0.3 grams	9
123.1090146	135.1670825	147.2251505	0.3 grams	14
132.6338564	144.6107149	156.5875734	0.3 grams	15
101.7734895	115.8362419	129.8989943	0.3 grams	17
55.70873986	60.63952039	65.57030093	0.3 grams	18
46.50958908	50.56190985	54.61423063	0.3 grams	20
50.12441103	51.24906216	52.3737133	0.3 grams	22
51.74128633	54.30641328	56.87154023	0.3 grams	24
21.34400829	41.15868661	60.97336493	0.3 grams	27
39.64654628	56.78818412	73.92982196	0.3 grams	29
31.27356289	45.36101477	59.44846665	0.3 grams	31
29.15591816	38.49257701	47.82923585	0.3 grams	33

Appendix II: Clay Bacteria Order Diversity

Values represent percentage abundances of each order within each sample, as measured by Research and Testing Laboratory (Lubbock, Texas).

Order Name	Illite Dry	Illite Sediment	Illite Water	Kaolinite Dry	Kaolinite Sediment	Kaolinite Water
Desulfovibrionales	0.0000	0.8735	0.0851	0.0000	17.2360	0.4263
Pseudomonadales	0.0000	3.1024	1.1917	0.4911	0.1046	1.8238
Clostridiales	38.6927	15.8735	5.9925	35.2363	9.5504	3.5291
Flavobacteriales	0.0000	0.4518	1.7194	0.0000	0.0000	0.0474
Rhodobacterales	0.8111	31.5361	52.6558	0.0000	44.7717	67.2430
Rhodospirillales	0.8588	2.9518	1.2598	0.3683	1.3942	2.4633
Bacillales	2.5763	33.6747	12.0872	16.4518	0.2963	0.1895
Rhizobiales	1.5744	0.5120	1.1236	2.3327	0.5751	3.2923
Oceanospirillales	0.0000	0.0904	0.0511	0.0000	8.5221	12.9086
Kordiimonadales	0.0000	0.0000	0.0170	0.0000	4.3046	0.1184
Vibrionales	0.0000	0.0000	0.0000	0.0000	0.0000	0.1184
Thermoanaerobacterales	0.9542	0.0602	0.0340	0.0000	2.5096	6.3240
Sphingomonadales	1.4790	0.7530	3.8645	1.3505	0.1568	1.0895
Thermales	0.0000	0.0000	0.0000	0.0000	0.1917	0.0711
Burkholderiales	1.6221	0.0000	0.0340	2.9466	0.0174	0.0711
Enterobacterales	0.0000	0.0000	0.0340	0.6139	0.0000	0.0947
Alteromonadales	0.0000	6.2349	0.2383	0.0000	0.6100	0.1895
Solirubrobacterales	11.2595	0.1205	0.0000	0.9822	0.0000	0.0000
Desulfobacterales	0.0000	1.2651	17.4498	0.0000	0.0000	0.0000
Planctomycetales	0.0000	0.5120	0.0340	0.1842	0.0000	0.0000
Cytophagales	0.1431	0.0301	0.0170	0.0000	0.0000	0.0000
Verrucomicrobiales	0.0000	0.2108	0.0000	0.0000	0.0000	0.0000
Haloplasmatales	0.0000	1.1145	0.8342	0.0000	0.0000	0.0000
Halanaerobiales	0.0000	0.2410	0.2554	0.0000	0.0000	0.0000
Bacteroidales	0.1431	0.1205	0.0000	3.9288	0.0000	0.0000
Actinomycetales	20.4198	0.2410	0.5107	5.2793	1.4814	0.0000
Ktedonobacterales	0.4294	0.0301	0.0000	0.0000	0.0000	0.0000
Desulfuromonadales	0.0000	0.0000	0.1192	0.4911	0.0000	0.0000
Neisseriales	0.0000	0.0000	0.0340	0.1228	0.0000	0.0000
Fusobacteriales	0.0000	0.0000	0.0000	3.8674	0.1394	0.0000
Gammaproteobacteria (order)	0.0000	0.0000	0.0000	0.0000	6.3437	0.0000
Chromatiales	0.0000	0.0000	0.0000	0.5525	1.7602	0.0000
Legionellales	0.0000	0.0000	0.0000	0.0000	0.0174	0.0000
Lactobacillales	0.0477	0.0000	0.1021	4.9724	0.0000	0.0000
Thermomicrobiales	0.8111	0.0000	0.0681	0.0000	0.0000	0.0000
Thiotrichales	0.0000	0.0000	0.0000	0.0000	0.0174	0.0000
Parvularculales	0.0954	0.0000	0.0170	0.0000	0.0000	0.0000
Sphaerobacterales	0.6202	0.0000	0.0511	0.0000	0.0000	0.0000
Erysipelotrichales	0.0000	0.0000	0.0511	16.3290	0.0000	0.0000

Xanthomonadales	0.4771	0.0000	0.0681	0.0000	0.0000	0.0000
Selenomonadales	10.2576	0.0000	0.0000	1.1664	0.0000	0.0000
Spartobacteria (order)	0.3340	0.0000	0.0000	0.0000	0.0000	0.0000
Acidobacteriales	2.1469	0.0000	0.0000	0.4297	0.0000	0.0000
Rubrobacterales	0.1908	0.0000	0.0000	0.0000	0.0000	0.0000
Acidimicrobiales	0.5725	0.0000	0.0000	0.0000	0.0000	0.0000
Opitutales	0.0954	0.0000	0.0000	0.0000	0.0000	0.0000
Coriobacteriales	0.0000	0.0000	0.0000	0.9822	0.0000	0.0000
Gemmatimonadales	0.0954	0.0000	0.0000	0.0000	0.0000	0.0000
Thermoleophilales	0.3817	0.0000	0.0000	0.0000	0.0000	0.0000
Caldilineales	0.2385	0.0000	0.0000	0.0000	0.0000	0.0000
Chloroflexales	0.5725	0.0000	0.0000	0.0000	0.0000	0.0000
Rhodocyclales	0.1431	0.0000	0.0000	0.0000	0.0000	0.0000
Nitrospirales	0.2863	0.0000	0.0000	0.0000	0.0000	0.0000
Nitrosomonadales	1.0019	0.0000	0.0000	0.1228	0.0000	0.0000
Oscillatoriales	0.0954	0.0000	0.0000	0.0000	0.0000	0.0000
Caulobacterales	0.1908	0.0000	0.0000	0.7366	0.0000	0.0000
Holophagales	0.1431	0.0000	0.0000	0.0000	0.0000	0.0000
Myxococcales	0.0954	0.0000	0.0000	0.0000	0.0000	0.0000
Betaproteobacteria (order)	0.0477	0.0000	0.0000	0.0000	0.0000	0.0000
Pasteurellales	0.0000	0.0000	0.0000	0.0614	0.0000	0.0000
Dehalococcoidales	0.0954	0.0000	0.0000	0.0000	0.0000	0.0000

Appendix III: Poster Presentation

Presented at the GSA Annual Meeting, October 2013.

Laboratory testing of the influence of substrate on decay inhibition and exceptional preservation

Victoria E. McCoy¹, Robert T. Young¹, and Derek E.G. Briggs²

¹Department of Geology and Geophysics, Yale University

²Department of Geology and Geophysics & Peabody Museum of Natural History, Yale University

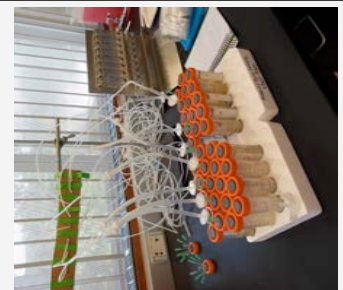


1. Introduction

Exceptional fossilization requires the inhibition of decay and/or the promotion of mineralization. Substrate permeability (Gaines et al., 2005; 2012) and chemistry (Butterfield, 1995) are hypothesized as controlling these factors, and were experimentally modeled here in order to test their effects on organic preservation.

2. Methods

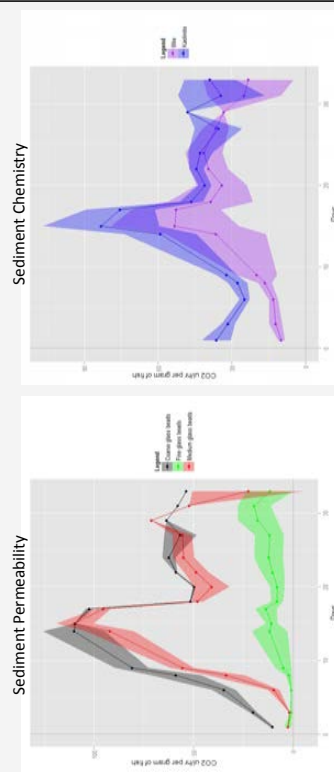
1. Cod tissue in five substrates: three sizes of glass beads; illite; kaolinite.
2. Infrared gas analysis (IRGA): measured carbon dioxide emission; proxy for decay.
3. Micro-CT scanning: revealed mineral precipitation.



3a. IRGA Results

Sediment permeability: higher permeability replicates (larger grain size) emitted more carbon dioxide than lower permeability replicates (smaller grain size), peaking earlier.

Sediment chemistry: kaolinite replicates emitted more carbon dioxide than illite replicates, peaking simultaneously.



3b. Bacteria Results

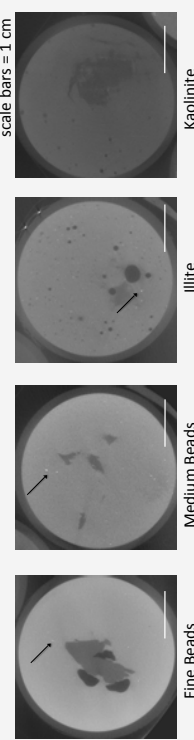
Different colors of bacterial growth in kaolinite and illite suggests the development of different microfaunas.

Microbial diversity analyses pending.



3c. Micro-CT Scanning Results

No soft tissue mineralization. Mineral precipitation within sediment in the fine beads, medium beads and illite. No mineral precipitation in coarse beads or kaolinite.



4. Conclusions

Preservation potential maximized by low permeability sediments.

Different chemical environments foster specific decay microenvironments.

No soft tissue mineralization, but **negative association between organic decay and mineral precipitation** suggests general trend.

5. Acknowledgements

Thanks to NEGS, Paleontological Society, NSF GRFP, Kennedy T Friend Association, Dr. Mark Bradford and lab, Dr. Zhenjiang, Dr. Jordan Peccia and lab, Dr. Zhen Zhuang, and Dr. Gerald Conlogue and lab.